

**PROPERTIES OF FLUORINE-INCORPORATED  
SILICON OXIDE FILMS AND EFFECTS OF  
PHOTON RADIATION DURING PECVD**

**By**

**Baldwin Pok Man Lam**

A Thesis  
Submitted to the Faculty of Graduate Studies  
in Partial Fulfillment of the Requirements  
for the Degree of

**Master of Science**

Department of Electrical & Computer Engineering  
University of Manitoba  
Winnipeg, Manitoba  
Canada

© July, 1995



National Library  
of Canada

Acquisitions and  
Bibliographic Services Branch

395 Wellington Street  
Ottawa, Ontario  
K1A 0N4

Bibliothèque nationale  
du Canada

Direction des acquisitions et  
des services bibliographiques

395, rue Wellington  
Ottawa (Ontario)  
K1A 0N4

*Your file* *Votre référence*

*Our file* *Notre référence*

The author has granted an irrevocable non-exclusive licence allowing the National Library of Canada to reproduce, loan, distribute or sell copies of his/her thesis by any means and in any form or format, making this thesis available to interested persons.

L'auteur a accordé une licence irrévocable et non exclusive permettant à la Bibliothèque nationale du Canada de reproduire, prêter, distribuer ou vendre des copies de sa thèse de quelque manière et sous quelque forme que ce soit pour mettre des exemplaires de cette thèse à la disposition des personnes intéressées.

The author retains ownership of the copyright in his/her thesis. Neither the thesis nor substantial extracts from it may be printed or otherwise reproduced without his/her permission.

L'auteur conserve la propriété du droit d'auteur qui protège sa thèse. Ni la thèse ni des extraits substantiels de celle-ci ne doivent être imprimés ou autrement reproduits sans son autorisation.

ISBN 0-612-13277-3

Canada

Name \_\_\_\_\_

*Dissertation Abstracts International* is arranged by broad, general subject categories. Please select the one subject which most nearly describes the content of your dissertation. Enter the corresponding four-digit code in the spaces provided.

Electrical Engineering

SUBJECT TERM

0544

U·M·I

SUBJECT CODE

**Subject Categories**

**THE HUMANITIES AND SOCIAL SCIENCES**

**COMMUNICATIONS AND THE ARTS**

Architecture	0729
Art History	0377
Cinema	0900
Dance	0378
Fine Arts	0357
Information Science	0723
Journalism	0391
Library Science	0399
Mass Communications	0708
Music	0413
Speech Communication	0459
Theater	0465

**EDUCATION**

General	0515
Administration	0514
Adult and Continuing	0516
Agricultural	0517
Art	0273
Bilingual and Multicultural	0282
Business	0688
Community College	0275
Curriculum and Instruction	0727
Early Childhood	0518
Elementary	0524
Finance	0277
Guidance and Counseling	0519
Health	0680
Higher	0745
History of	0520
Home Economics	0278
Industrial	0521
Language and Literature	0279
Mathematics	0280
Music	0522
Philosophy of	0998
Physical	0523

Psychology	0525
Reading	0535
Religious	0527
Sciences	0714
Secondary	0533
Social Sciences	0534
Sociology of	0340
Special	0529
Teacher Training	0530
Technology	0710
Tests and Measurements	0288
Vocational	0747

**LANGUAGE, LITERATURE AND LINGUISTICS**

Language	
General	0679
Ancient	0289
Linguistics	0290
Modern	0291
Literature	
General	0401
Classical	0294
Comparative	0295
Medieval	0297
Modern	0298
African	0316
American	0591
Asian	0305
Canadian (English)	0352
Canadian (French)	0355
English	0593
Germanic	0311
Latin American	0312
Middle Eastern	0315
Romance	0313
Slavic and East European	0314

**PHILOSOPHY, RELIGION AND THEOLOGY**

Philosophy	0422
Religion	
General	0318
Biblical Studies	0321
Clergy	0319
History of	0320
Philosophy of	0322
Theology	0469

**SOCIAL SCIENCES**

American Studies	0323
Anthropology	
Archaeology	0324
Cultural	0326
Physical	0327
Business Administration	
General	0310
Accounting	0272
Banking	0770
Management	0454
Marketing	0338
Canadian Studies	0385
Economics	
General	0501
Agricultural	0503
Commerce-Business	0505
Finance	0508
History	0509
Labor	0510
Theory	0511
Folklore	0358
Geography	0366
Gerontology	0351
History	
General	0578

Ancient	0579
Medieval	0581
Modern	0582
Black	0328
African	0331
Asia, Australia and Oceania	0332
Canadian	0334
European	0335
Latin American	0336
Middle Eastern	0333
United States	0337
History of Science	0585
Law	0398
Political Science	
General	0615
International Law and Relations	0616
Public Administration	0617
Recreation	0814
Social Work	0452
Sociology	
General	0626
Criminology and Penology	0627
Demography	0938
Ethnic and Racial Studies	0631
Individual and Family Studies	0628
Industrial and Labor Relations	0629
Public and Social Welfare	0630
Social Structure and Development	0700
Theory and Methods	0344
Transportation	0709
Urban and Regional Planning	0999
Women's Studies	0453

**THE SCIENCES AND ENGINEERING**

**BIOLOGICAL SCIENCES**

Agriculture	
General	0473
Agronomy	0285
Animal Culture and Nutrition	0475
Animal Pathology	0476
Food Science and Technology	0359
Forestry and Wildlife	0478
Plant Culture	0479
Plant Pathology	0480
Plant Physiology	0817
Range Management	0777
Wood Technology	0746
Biology	
General	0306
Anatomy	0287
Biostatistics	0308
Botany	0309
Cell	0379
Ecology	0329
Entomology	0353
Genetics	0369
Limnology	0793
Microbiology	0410
Molecular	0307
Neuroscience	0317
Oceanography	0416
Physiology	0433
Radiation	0821
Veterinary Science	0778
Zoology	0472
Biophysics	
General	0786
Medical	0760

Geodesy	0370
Geology	0372
Geophysics	0373
Hydrology	0388
Mineralogy	0411
Paleobotany	0345
Paleoecology	0426
Paleontology	0418
Paleozoology	0985
Palynology	0427
Physical Geography	0368
Physical Oceanography	0415

**HEALTH AND ENVIRONMENTAL SCIENCES**

Environmental Sciences	0768
Health Sciences	
General	0566
Audiology	0300
Chemotherapy	0992
Dentistry	0567
Education	0350
Hospital Management	0769
Human Development	0758
Immunology	0982
Medicine and Surgery	0564
Mental Health	0347
Nursing	0569
Nutrition	0570
Obstetrics and Gynecology	0380
Occupational Health and Therapy	0354
Ophthalmology	0381
Pathology	0571
Pharmacology	0419
Pharmacy	0572
Physical Therapy	0382
Public Health	0573
Radiology	0574
Recreation	0575

Speech Pathology	0460
Toxicology	0383
Home Economics	0386

**PHYSICAL SCIENCES**

Pure Sciences	
Chemistry	
General	0485
Agricultural	0749
Analytical	0486
Biochemistry	0487
Inorganic	0488
Nuclear	0738
Organic	0490
Pharmaceutical	0491
Physical	0494
Polymer	0495
Radiation	0754
Mathematics	0405
Physics	
General	0605
Acoustics	0986
Astronomy and Astrophysics	0606
Atmospheric Science	0608
Atomic	0748
Electronics and Electricity	0607
Elementary Particles and High Energy	0798
Fluid and Plasma	0759
Molecular	0609
Nuclear	0610
Optics	0752
Radiation	0756
Solid State	0611
Statistics	0463

**Applied Sciences**

Applied Mechanics	0346
Computer Science	0984

Engineering	
General	0537
Aerospace	0538
Agricultural	0539
Automotive	0540
Biomedical	0541
Chemical	0542
Civil	0543
Electronics and Electrical	0544
Heat and Thermodynamics	0348
Hydraulic	0545
Industrial	0546
Marine	0547
Materials Science	0794
Mechanical	0548
Metallurgy	0743
Mining	0551
Nuclear	0552
Packaging	0549
Petroleum	0765
Sanitary and Municipal	0554
System Science	0790
Geotechnology	0428
Operations Research	0796
Plastics Technology	0795
Textile Technology	0994

**PSYCHOLOGY**

General	0621
Behavioral	0384
Clinical	0622
Developmental	0620
Experimental	0623
Industrial	0624
Personality	0625
Physiological	0989
Psychobiology	0349
Psychometrics	0632
Social	0451



PROPERTIES OF FLUORINE-INCORPORATED SILICON OXIDE  
FILMS AND EFFECTS OF PHOTON RADIATION  
DURING PECVD

BY

BALDWIN POK MAN LAM

A Thesis submitted to the Faculty of Graduate Studies of the University of Manitoba  
in partial fulfillment of the requirements of the degree of

MASTER OF SCIENCE

© 1995

Permission has been granted to the LIBRARY OF THE UNIVERSITY OF MANITOBA  
to lend or sell copies of this thesis, to the NATIONAL LIBRARY OF CANADA to  
microfilm this thesis and to lend or sell copies of the film, and LIBRARY  
MICROFILMS to publish an abstract of this thesis.

The author reserves other publication rights, and neither the thesis nor extensive  
extracts from it may be printed or other-wise reproduced without the author's written  
permission.

I hereby declare that I am the sole author of this thesis.

I authorize the University of Manitoba to lend this thesis to other institutions or individuals for the purpose of scholarly research.

Baldwin Pok Man Lam

I further authorize the University of Manitoba to reproduce this thesis by photocopying or by other means, in total or in part, at the request of other institutions or individuals for the purpose of scholarly research.

Baldwin Pok Man Lam

## ABSTRACT

The physical properties of the SiOF films and the effects of photon radiation on the SiO<sub>2</sub> films have been experimentally studied. The films used for the MOS devices were fabricated by ECR microwave PECVD process at 305°C. The FTIR and XPS spectra were used to characterize the SiOF films. The results show that fluorine incorporation enhances the film deposition rate for the flow rate of fluorine below 6 sccm, and etches the films if the flow rate is greater than 6 sccm. The breaking of the strained Si-O-Si bonds and the formation of Si-F bonds by fluorine incorporation induce stress relaxation. The XPS spectra confirm that fluorine is bonded to silicon but not to oxygen in the SiOF films. There is a desorption of atomic fluorine after heat treatment at 400, 500 and 600°C. A charged particle suppressor has been designed for the study of the effects of photon radiation. With this suppressor, a suitable dc biasing applied to the grids suppresses all charged particles and thus enables exhibition of the role played by photons. For the photons produced by the N<sub>2</sub>O plasma at 10<sup>-3</sup> mTorr, the photon radiation causes an increase in both the interface trap concentration from 6 x 10<sup>11</sup> eV<sup>-1</sup> cm<sup>-2</sup> to 10<sup>12</sup> eV<sup>-1</sup> cm<sup>-2</sup> and the oxide trapped charge from 10<sup>11</sup> q cm<sup>-2</sup> to 4.5 x 10<sup>11</sup> q cm<sup>-2</sup> for MOS devices after post metallization annealing (PMA).

## ACKNOWLEDGMENTS

The author would like to thank his advisor, Dr. K. C. Kao for his valuable advice, guidance, assistance and patience throughout the development of this thesis. The author is also indebted to his colleagues of the Materials and Devices Research Laboratory, in particular, T. T. Chau, for their technical assistance and helpful discussions.

The author would like to dedicate this thesis to his parents and younger sister for their continuous encouragement, support and understanding.

Last but not the least, the author would also like to thank Yi for her support and understanding throughout the period of preparation of this thesis.

The financial support of the Natural Sciences and Engineering Research Council of Canada for this research is also gratefully acknowledged.

# TABLE OF CONTENTS

<b>Abstract</b>	iii
<b>Acknowledgments</b>	iv
<b>List of Figures</b>	vii
<b>List of Tables</b>	x
<b>1. Introduction</b>	1
<b>2. Review of the Properties of Fluorinated Silicon Oxide Films and the ECR Microwave Plasma Processing Techniques</b>	4
2.1 The Chemical Composition of SiOF Films	4
2.2 The Effects of Fluorine in the Silicon Oxide	8
2.3 ECR Microwave Processing	11
2.4 The Plasma Processing System and the Species Selector and Energy Controller (SSEC)	15
2.5 SiO <sub>2</sub> Films Fabricated by ECR Microwave Plasma	18
2.6 Forming Gas Annealing	20
2.6.1 Relaxation of Strained Bonds	21
2.6.2 Hydrogenation of Defects	21
<b>3. Fluorine-Incorporated Silicon Oxide Films Fabricated by ECR Microwave Plasmas</b>	24
3.1 Infrared Absorption Spectra	26
3.1.1 Dependence on the Flow Rate of CF <sub>4</sub> gas	28
3.1.2 Dependence on the Flow Rate of Oxygen gas	32
3.1.3 Dependence on the Flow Rate of Silane gas	35
3.2 Heat Treatment of SiOF Films	37
3.3 X-Ray Photoelectron Spectroscopy (XPS)	41
<b>4. The Photon Radiation Effects on the ECR Microwave PECVD SiO<sub>2</sub> Films</b>	45

4.1 Experimental Techniques and the Charged Particle Suppressor	45
4.2 Floating Potential	49
4.3 Ion and Electron Currents	50
4.4 Interface Trap Charge ( $D_{it}$ ) and Oxide Trapped Charge ( $Q_{ox}$ )	54
5. Conclusions	60
References	61
Appendix A (RCA Silicon Substrate Cleaning Process)	64
Appendix B (Capacitance-Voltage Method)	65

# LIST OF FIGURES

Figure	Page
2.1 Schematic representation of atomic arrangements in the outer region of the Si surface after (a) HF treatment, (b) oxidation, and (c) extended oxidation.	6
2.2 Schematic diagram showing (a) the thermal oxidation process for the fabrication of the SiO <sub>2</sub> films, and (b) the PECVD process for fabrication of SiO <sub>2</sub> films.	15
2.3 The ECR microwave plasma system.	16
2.4 Schematic diagram for the plasma and processing chambers and the position of the SSEC.	18
3.1 A typical FTIR spectrum of the SiOF films.	27
3.2 The deposition rate of SiOF films as a function of the flow rate of CF <sub>4</sub> gas with oxygen and silane gases at fixed flow rates of 10 and 1 sccm, respectively.	30
3.3 The refractive index of SiOF films as a function of the flow rate of CF <sub>4</sub> gas with oxygen and silane gases at fixed flow rates of 10 and 1 sccm, respectively.	31
3.4 The wavenumber for the occurrence of the Si-O-Si stretching peak of SiOF films as a function of the flow rate of CF <sub>4</sub> gas with oxygen and silane gases at fixed flow rates of 10 and 1 sccm, respectively.	31
3.5 FWHM (a) and the SiF/Si-O-Si stretching absorption peak ratio (b) of SiOF films as a function of the flow rate of CF <sub>4</sub> gas with oxygen and silane gases at fixed flow rates of 10 and 1 sccm, respectively.	32

- 3.6** Deposition rate (a) and refractive index (b) of SiOF films as functions of the flow rate of oxygen gas with both silane and CF<sub>4</sub> flow rates at 1 sccm. 33
- 3.7** Wavenumber for the occurrence of the Si-O-Si stretching peak of SiOF films as a function of the flow rate of oxygen gas with both silane and CF<sub>4</sub> flow rates at 1 sccm. 33
- 3.8** SiF/Si-O-Si absorption peak ratio of SiOF films as a function of the flow rate of oxygen gas with both silane and CF<sub>4</sub> flow rates at 1 sccm. 34
- 3.9** Deposition rate of SiOF films as a function of the flow rate of silane gas with the oxygen and CF<sub>4</sub> gases kept at constant flow rates of 20 and 1 sccm, respectively. 36
- 3.10** Refractive index (a) and wavenumber for the occurrence of the Si-O-Si stretching absorption peak (b) of SiOF films as functions of the flow rate of silane gas with the oxygen and CF<sub>4</sub> gases kept at constant flow rates of 20 and 1 sccm, respectively. 36
- 3.11** SiF/Si-O-Si absorption peak ratio of SiOF films as a function of the flow rate of silane gas with the oxygen and CF<sub>4</sub> gases kept at constant flow rates of 20 and 1 sccm, respectively. 37
- 3.12** SiF/Si-O-Si absorption peak ratio as a function of heat treatment temperature for the SiOF samples (A) O<sub>2</sub> : 10 sccm, SiH<sub>4</sub> : 1 sccm, CF<sub>4</sub>: 1 sccm; (B) O<sub>2</sub> : 10 sccm, SiH<sub>4</sub> : 1 sccm, CF<sub>4</sub>: 4 sccm; (C) O<sub>2</sub> : 10 sccm, SiH<sub>4</sub> : 1 sccm, CF<sub>4</sub>: 10 sccm. 39
- 3.13** Wavenumber for the occurrence of Si-O-Si stretching absorption peak as a function of heat treatment temperature for SiOF samples (A) O<sub>2</sub> : 10 sccm, SiH<sub>4</sub> : 1 sccm, CF<sub>4</sub>: 1 sccm; (B) O<sub>2</sub> : 10 sccm, SiH<sub>4</sub> : 1 sccm, CF<sub>4</sub>: 4 sccm; (C) O<sub>2</sub> : 10 sccm, SiH<sub>4</sub> : 1 sccm, CF<sub>4</sub>: 10 sccm. 40
- 3.14** The XPS spectra of the SiOF film fabricated in a gas mixture of CF<sub>4</sub>, O<sub>2</sub> and SiH<sub>4</sub> at flow rates of 10, 10 and 1 sccm, respectively. 43

4.1	Schematic diagram of the charged particle suppressor.	46
4.2	Experimental arrangement for the measurements of ion and electron currents from the N <sub>2</sub> O plasma.	48
4.3	The floating potentials induced by the N <sub>2</sub> O plasma (10 sccm) at the front and the back grids.	50
4.4	Ion and electron currents of the N <sub>2</sub> O plasma as functions of pressure without external bias (Arrangement A).	52
4.5	Ion and electron N <sub>2</sub> O plasma as functions of pressure with external bias voltages of -25 V at the front grid and 25 V at the back grid (Arrangement B).	52
4.6	Ion and electron currents N <sub>2</sub> O plasma as functions of pressure with external bias voltages of -40 V at the front grid and 40 V at the back grid (Arrangement E).	53
4.7	The Bond Strain Gradient model showing the rupture of the Si-O bond and the subsequent propagation of the defects toward the SiO <sub>2</sub> /Si interface.	57
4.8	Illustration of the flow of particles and photons between the plasma and processing chamber with no bias.	59

## LIST OF TABLES

Table	Page
2.1 Bond energies of molecules involved in fluorine-incorporated silicon oxide films.	6
3.1 The gas flow rates used for fabrication of SiOF films.	25
3.2 The identification of different absorption peaks in SiOF films.	27
3.3 The gas mixture used for fabrication of the SiOF samples for heat treatment experiments.	38
3.4 Composition in atomic % of the SiOF films fabricated at gas flow rates of $\text{CF}_4 : \text{O}_2 : \text{SiH}_4 = 10 : 10 : 1$ sccm.	42
3.5 Binding energies of Si, C, O and F in SiOF films.	44
4.1 The biasing arrangements for the measurements of electron and ion currents induced by the $\text{N}_2\text{O}$ plasma.	51
4.2 The values of $D_{it}$ and $Q_{ox}$ before and after photon radiation.	55

# CHAPTER 1

## INTRODUCTION

Silicon dioxide has become the most common gate insulating material. With device geometries scaled to increase circuit density, new processing techniques and new materials have been introduced to obtain finer geometries and interconnections with lower resistivity. In addition, in device-switching performance, the interconnection delay has become important, which is mainly caused by the large parasitic capacitance in interconnections. Therefore, the capacitance in interconnections should be reduced in order to achieve high-performance VLSI devices. A trend to improve the properties mentioned above is the incorporation of fluorine to silicon dioxide during oxidation.

Previous works have shown that introducing a small amount of fluorine into oxygen during thermal oxidation would significantly improve the properties of MOS devices [1-9]. The specific improvement includes a significant suppression of hot electron induced interface traps [2]. The effects of fluorine incorporation on the dielectric breakdown strength [8], the radiation response [2, 6], and the relative dielectric constant of the silicon oxide films have also been investigated.

There are a number of ways to introduce fluorine into the silicon dioxide, such as diffusion [2-5, 8], ion implantation [6] and pre-oxidation HF treatment [1, 6]. In our laboratory, we used electron cyclotron resonance (ECR) microwave plasma processing with  $\text{CF}_4$  incorporation in the deposition of the  $\text{SiO}_2$  films. One of the objectives of this research is to study the physical properties of the fluorine-incorporated  $\text{SiO}_2$  films deposited by this method.

The plasma-enhanced chemical vapor deposition (PECVD) is a low-temperature processing (about  $300^\circ\text{C}$  to  $400^\circ\text{C}$ ) [26, 27, 30, 32]. To minimize the diffusion-related and high-temperature sensitive effects which may seriously affect the performance of small

MOS devices, several techniques based on this concept have been reported recently, and each technique has its own advantages and disadvantages. The radio frequency (rf) PECVD technique has a high deposition rate but it also has some drawbacks. It suffers radiation and ion bombardment damage during deposition of the films. Another PECVD technique is the ECR microwave PECVD, which requires a higher carrier gas flow and a lower operating pressure (in the order of mTorr). This results in a lower deposition rate and the deposited films may suffer vacuum UV radiation damage. However, a downstream ECR microwave PECVD technique can reduce the UV radiation damage but it suffers from the formation of microdust and the bombardment of energetic particles (mainly ions) on the substrates and the on-growing films during the PECVD process.

In order to deposit good quality PECVD SiO<sub>2</sub> films, three conditions must be met [26]:

- (1) The PECVD system must prevent the back-diffusion of SiH<sub>4</sub> from entering the plasma region in order to reduce the heterogeneous gas-phase reaction due to the discharge of SiH<sub>4</sub> to form microdust particles in the plasma chamber.
- (2) The system must suppress all of the energetic particles (electrons, ions and photons) from bombarding the substrates and the on-growing films in order to reduce the damage on the SiO<sub>2</sub>/Si interface and defects in the bulk of the films.
- (3) The system must provide sufficient activated species for the chemical reaction taking place at the substrate surface in order to maintain a good reaction rate for the formation of the films.

To meet these three conditions, one approach is to separate the plasma volume from the substrates. The Materials and Devices Research group at the *University of Manitoba* has developed an apparatus called the species selector and energy controller (SSEC) [26] to separate the plasma source from the processing chamber. The basic function of this apparatus is to reduce the energy of plasma-generated species by making them to scatter with the walls of the SSEC before they enter the processing chamber. In

order to further minimize the damage caused by ion bombardment, the SSEC has been modified to enable the use of dc biasing for controlling the energies of the charges particles. The SSEC can block completely the photon radiation from the plasma to the substrates. Although many investigators have realized the damaging effects of photon radiation, the experimental data about these effects are not available. Therefore, another objective of this research is to study how much the photon radiation would affect the properties of the MOS devices.

In this thesis, a brief review of the properties of the fluorinated silicon oxide and also the principle of the ECR microwave PECVD technique with the apparatus of SSEC are given in Chapter 2. The experimental methods for producing fluorinated  $\text{SiO}_2$  films and their properties are described in Chapter 3. The apparatus developed for the study of the photon radiation effects and some preliminary results are given in Chapter 4. On the basis of all experimental results, conclusions are drawn and given in Chapter 5.

## CHAPTER 2

# REVIEW OF THE PROPERTIES OF FLUORINATED SILICON OXIDE FILMS AND THE ECR MICROWAVE PLASMA PROCESSING TECHNIQUES

The introduction of halogen atoms into the oxidizing gas stream during deposition of silicon oxide films would result in a marked enhancement of the deposition rate and a significant improvement in electric properties of the oxide and of the oxide/silicon interface. Chlorine-related effects on MOS devices, such as the deposition rate enhancement, the mobile ion gettering, and the increase of minority carrier lifetime, have been investigated since the early 1970's. It has been shown that MOS devices with improved electrical properties including a better threshold stability can be achieved by the incorporation of fluorine in silicon oxide films.

Within a broader context of halogen oxidation as a means of growing silicon oxide films with improved properties to be used in VLSI fabrication, the incorporation of fluorine in the MOS devices has recently become of interest to industry. It has been known since 1980's that the effect of fluorine on the oxidation rate is much more pronounced than the corresponding chlorine and, in addition, fluorine can also induce a marked oxide relaxation [6]. This effect can be attributed to the reduction of the bond strain gradient and the passivation of dangling silicon bonds by fluorine.

### 2.1 The Chemical Composition of SiOF Films

Fluorine can be incorporated in silicon oxide bulk and at the silicon oxide/silicon interface in a number of ways. Some of these are HF treatment before oxidation, anodic oxidation in a fluorinated electrolyte,  $\text{NF}_3$  enhanced oxidation, ion implantation, plasma-enhanced chemical vapor deposition (PECVD) with  $\text{CF}_4$  inclusion,

etc. Of these methods,  $\text{NF}_3$  enhanced oxidation and fluorine implantation are two of the most commonly used methods.

Previous works [1-20, 22-25, 28-30] have shown that the fluorinated oxide has significant improvement in oxidation rate, stress relaxation and electrical properties, etc. There is clearly a change in the bonding structure of silicon oxide with the incorporation of fluorine. A two-step model has been put forward to explain the bonding structure in the fluorinated oxide. First, a fluorine atom diffuses and bonds to a dangling bond, or a weakened bond in the silicon oxide. The fluorine atoms will then accumulate and break the Si-O-Si bonds. The X-ray photoelectron spectroscopy (XPS) has revealed that fluorine atoms in the silicon oxide primarily bond to silicon atoms to form Si-F bonds but not to oxygen [12, 17, 23, 30], which causes changes in the local microstructure of the oxide [20], and hence facilitates a fast diffusion of both oxygen and fluorine through the oxide towards the silicon oxide/silicon interface. The extra Si dangling bonds (broken by fluorine) are then available to react with oxygen to form another Si-O-Si bond.

It should be noted that the incorporation of fluorine by HF treatment results in the Si-O-F bonding, possibly due to oxygen insertion into Si-F bond to form oxyfluoride moieties [50]. This sequence of chemical changes during the oxidation process is illustrated in Fig. 2.1(a) - (c) [50]. Initially, HF treatment results in the formation of a surface layer of hydrogen while fluorine has a broad subsurface distribution as shown in Fig. 2.1(a). When the HF-treated sample is oxidized, reactive oxygen attacks the Si-H and Si-F bonds forming bridged and non-bridged SiO structures and incorporating H and F into hydroxyl (-OH) and oxyfluoride (-OF) moieties as shown in Fig. 2.1(b). The layer of OF and OH bondings become the interface of the growing oxide, and further oxidation will involve migration of oxygen through the fluorinated oxide to consume a new silicon layer as shown in Fig. 2.1(c).

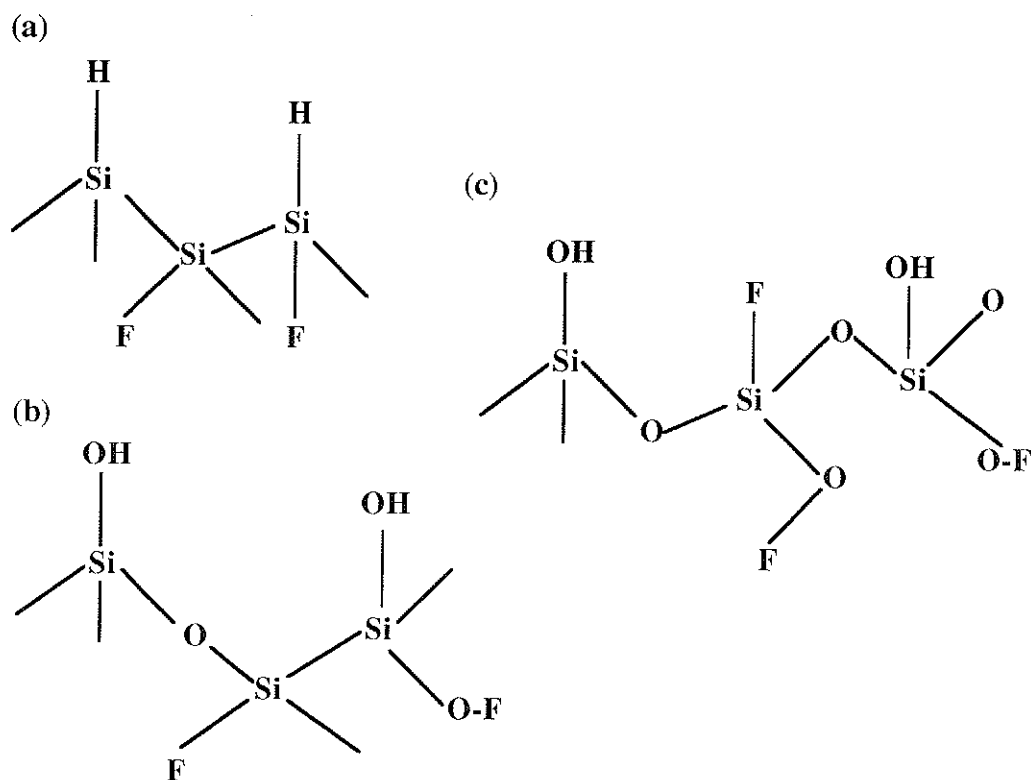


Figure 2.1 Schematic representation of the atomic arrangements in the outer region of the Si surface after (a) HF treatment, (b) oxidation, and (c) extended oxidation.

There are two key roles of fluorine in SiO<sub>2</sub> films:

- (1) the replacement of Si-H (or Si-OH) bonds by the much stronger Si-F bonds, and
- (2) the breaking of the strained Si-O-Si bonds by forming Si-F and O-Si bonds, resulting in stress relaxation. The bond energies of the elements involved in fluorinated silicon oxide are given in Table 2.1 [20].

Table 2.1 Bond energies of molecules involved in fluorine-incorporated silicon oxide films.

Bond Elements	Bond Energy (eV)
F-F	1.6
Si-Si	1.9
O-F	2.1
N-F	2.8
Si-O	4.5
Si-F	5.8

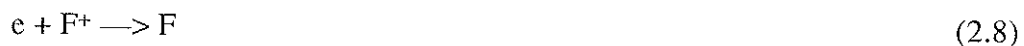
Halogens have been known as 'catalyst' of dielectric films to increase the oxidation or the deposition rate and halogens can also improve the various electrical characteristics of MOS devices. The interaction of fluorine with silicon oxide is much more pronounced than that of chlorine because fluorine has a higher electronegativity, which results in a marked oxidation stress relaxation [6, 18]. There are a variety of fluorine containing compounds, such as  $\text{XeF}_2$ ,  $\text{SiF}_4$ , atomic and molecular fluorine,  $\text{SiF}_4$  sputtered amorphous silicon,  $\text{SF}_6$  plasma and  $\text{CF}_4$  plasma, which can be used for the incorporation of fluorine into silicon oxide. However,  $\text{CF}_4$  has been used extensively in Si and  $\text{SiO}_2$  etching. Incorporation of a small amount of oxygen in the  $\text{CF}_4$  plasma can increase the amount of atomic fluorine [44]. It is believed that the oxygen species react with the  $\text{CF}_x$  species to release fluorine. The formation of the SiOF films is usually carried out by a PECVD process.

In the  $\text{CF}_4$  plasma, the energy of electrons is larger than those of ions and neutral particles (thermal non-equilibrium state). Although the energies of the ions and neutral particles are relatively low, they can be excited by the collision with electrons. The excited state is equivalent to a high-temperature-induced activation, and the effective reaction can thus proceed at a lower temperature. After being excited in the form of plasma,  $\text{CF}_4$  will be decomposed into  $\text{CF}_3$ ,  $\text{CF}_2$ ,  $\text{CF}$ , and atomic fluoride.



In the absence of oxygen, electrons in the discharge may decompose  $\text{CF}_4$  via the following reactions [44]:





In the discharge without oxygen, reactions (2.5) and (2.6) together with the detachment reaction (2.8) are apt to be the principal source of fluorine atoms. When oxygen is added to the  $CF_4$  plasma, the fluorine atom concentration is increased significantly [45]. The role of oxygen in fluorocarbon glow discharge is to react with carbon to form  $CO$ ,  $CO_2$ , or  $COF_2$  [45], thus increasing the effective fluorine atom concentration. There are several plausible explanations for the increase in fluorine atom concentration due to the added oxygen [44], and they are:

- (1) Oxygen retards the heterogeneous recombination of fluorine atoms with other species either by reacting with them or by blocking access to a favorable recombination surface.
- (2) Oxygen retards the rate of the homogeneous reaction of fluorine atoms with other species by depleting the reactants via oxidation.
- (3) Oxygen retards the loss rate of fluorine such as  $F^-$  by removing species which would otherwise consume the precursors.
- (4) Oxygen reacts with fluorine-containing species to liberate fluorine atoms. The reaction may occur at the surface or in gas phase.

## 2.2 The Effects of Fluorine in the Silicon Oxide

The fluorinated oxides sustains much less hot-electron induced damage [1] and also exhibits an excellent stability under a high-field stress, especially when electrons are injected from the substrate [9]. Nishioka et al. [1] have reported that the incorporation of fluorine in the oxide substantially reduces the as-grown bond strain gradient near the silicon oxide/silicon interface (the strained Si-O-Si bonds are replaced by Si-F bonds) to a point

that it is overcome by the Al-gate induced strain gradient which is in the direction opposite to the as-grown gradient [52]. Therefore, according to the Bond Strain Gradient model [48], this would mean that the non-bridging oxygen defect, which could form interface traps when it migrates to the silicon oxide/silicon interface, would tend to move in the direction away from the interface. On the other hand, the prolonged  $\text{NF}_3$  purge (100ppm for more than 15 seconds) degrades the hot-electron hardness of the SiOF films [2], results in higher values of interface trap density ( $D_{it}$ ). Wright et al. [12] have also reported that interface trap density increases as the fluorine implant dose is higher than  $10^{15} \text{ cm}^{-2}$ . The degraded interface state hardness may indicate an increase in the defects, which suggests that oxygen deficiency of stretched Si-Si bonds exists due to excess fluorine incorporation.

The oxidation rate is enhanced by fluorine incorporation [1-9]. Fluorine can act catalytically at the interface and compete with oxygen to form Si-F bonds because fluorine has a higher electronegativity than oxygen. This increases the number of Si dangling bonds and increases the reactivity at the interface and subsequently the growth rate of the oxidation. Fluorine can also effectively substitute for oxygen as an oxide network modifier and thus open the structure to more readily allow ingress of the oxidant. This also directly relates to the change in the local stress and viscosity at the interface resulting in a lower refractive index. Another possible explanation is the formation of volatile molecules such as  $\text{SiF}_4$  caused by the direct reaction of  $\text{NF}_3$  with  $\text{SiO}_2$  surface [53]. In the contrast, the tetraethoxysilane (TEOS)-based PECVD fluorinated oxide which is controlled by the flow rate of  $\text{C}_2\text{F}_6$  gas, has a decreasing deposition rate as the flow rate of  $\text{C}_2\text{F}_6$  gas increases [30]. This would be due to the domination of the etching process, probably caused by the formation of HF from the reaction of fluorine with the residual moistures (i.e.,  $\text{H}_2\text{O}$ ). Therefore, the proper amount of fluorine incorporation is vital to the deposition or oxidation rate of the SiOF films.

The fluorine concentration is uniform throughout the oxide film in the  $\text{NF}_3$  enhanced oxidation at  $800^\circ\text{C}$  and  $900^\circ\text{C}$  [4]. However, at  $1000^\circ\text{C}$ , the fluorine

concentration level is no longer uniform but rises toward a prominent peak at the silicon oxide/silicon interface. More fluorine is incorporated in the oxide for the same flow rate of  $\text{NF}_3$  gas if the oxidation temperature is lower [4]. The higher flow rate of  $\text{NF}_3$  gas results in the same profile but with a higher overall fluorine concentration level. The deposition temperature dependence of the SiOF films suggests that a thermally activated chemical reaction replacing fluorine bonded in the oxide network takes place during the oxidation process. The fluorine released from this reaction diffuses away, either toward the interface to react and become bonded again, making fluorine concentration highest at the interface, or going out of the oxide. The out-diffusion explains why a lower overall level of fluorine concentration is observed at a higher oxidation temperature. Fluorine atoms moving towards the oxidizing interface are incorporated in the growing oxide network there, resulting in a fluorine concentration peak near the interface.

The interface trap density of the SiOF films increases with time at room temperature after irradiation [6]. Immediately after irradiation, a prominent peak of  $D_{it}$  appears at the energy level above the midgap of the SiOF films (peak-1). A thousand hours after irradiation, peak-1 decreases but another peak of  $D_{it}$  is built-up at an energy level below the midgap (peak-2). The rate of growth of peak-2 is correlated with the rate of decrease of peak-1. Some of the fluorine species, which are originally bonded to the  $\text{SiO}_2$  lattice, could be set free by the radiation and become highly chemically active and they may react with hydrogen to form HF. If this reaction takes place more readily than that between hydrogen and Si-H at the interface, the presence of fluorine near the interface would then act as a sink for the hydrogen species (e.g.,  $\text{H}^+$ ) arriving from the bulk, and suppress the evolution with time of interface traps due to the hydrogen ions [54].

Before annealing, the relative dielectric constant of the conventional tetraethoxysilane (TEOS)-based PECVD oxide is about 4.9 [30], which is higher than that of thermally grown  $\text{SiO}_2$  films (3.9). The higher dielectric constant in the PECVD oxide is due to the presence of high polarized compounds such as Si-OH and  $\text{H}_2\text{O}$  in the film. The

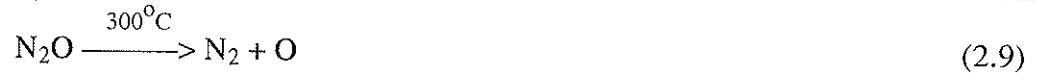
dielectric constant of the SiOF films decreases with increasing flow rate of fluorine gas, which is due to the breaking of Si-OH and O-H-O bonds by fluorine to form Si-F bonds. After annealing at 400°C, the dielectric constant of the SiOF film decreases. At 14 atomic percent of fluorine concentration in the SiOF films, the relative dielectric constant is 3.6, which is lower than that of thermally grown oxide.

### **2.3 ECR Microwave Plasma Processing**

In chemical vapor deposition (CVD), one or more gases react on the substrate surface to form a film. A CVD is a process to supply reactive gases to a substrate surface under conditions favorable to surface reaction but not favorable to reaction elsewhere. On the other hand, an efficient method for breaking gas molecules into reactive fragments is to make the gases electrically discharged to form a plasma. In a plasma reactants will be dissociated into fragments at substantially reduced temperatures and this is why it is called plasma-enhanced CVD.

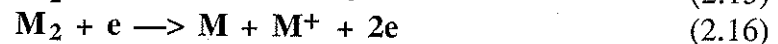
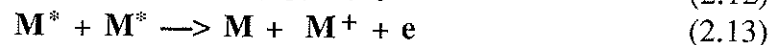
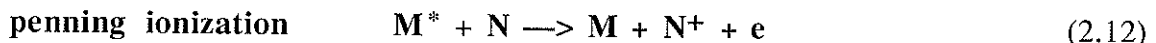
When a microwave plasma is subjected to an externally applied magnetic field perpendicular to the electric field vector of the electromagnetic excitation, electrons and ions are forced to assume circular or helical paths around the line of force of the magnetic field and hence the electrons and ions are confined in the direction perpendicular to the magnetic field vector. As the applied magnetic field is increased, the angular frequency of the electron rotation also increases and when this frequency reaches the angular frequency of the microwave electromagnetic excitation, the electron cyclotron resonance (ECR) condition sets in. Under this condition the energy required to excite or maintain the plasma is minimal [26].

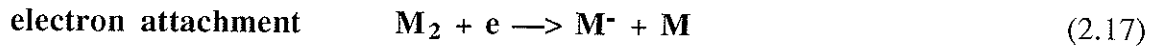
An ECR microwave PECVD process in a gas mixture of  $N_2O$  and  $SiH_4$  can be simply expressed as follows:



In the ECR microwave PECVD process, the microwave energy instead of the thermal energy is used to excite the gas. A plasma is a neutral ionized gas consisting of free electrons, ions, radicals, neutral and excited species, and photons. The neutral and excited species and radicals normally outnumber the electrons and ions and are not influenced by the external fields. Even in the plasma with a single gas, the number of dissociated species is enormous. Virtually any possible breakdown product of a gas, including both fragments and ions, would be present and play an important role in the physical and chemical properties of the plasma.

To maintain a plasma, a gas must receive a constant input of energy to offset the loss of the particles by recombination. It must also be kept at the same low pressure to maintain the same collision rate and thus the recombination rate of the ions. The formation of a plasma begins with some free electrons and an applied field sufficient to ionize the gas atoms. During impact ionization, the newly generated electrons are then accelerated by the applied field and collide with other particles to produce more electrons. The processes are shown as follows:





The electron energy in a plasma is much higher than the chemical bonding energy. Molecules in a plasma are essentially randomized and they break down after collision with electrons into all conceivable fragments. Energy releases as light (photon) due to recombination, giving plasma a characteristic diffuse glow.

A photon is an energy particle in the plasma. Recombination of electrons with positively charged ions, relaxation of excited ions and molecules, and ion and electron bombardments on any surface in the chamber may produce photons. The damage created by photons depends on their energy as well as the properties of the photon striking surface. In SiO<sub>2</sub> and at the SiO<sub>2</sub>/Si interface the photon-induced damage includes creation of interface states, fixed charges and neutral traps.

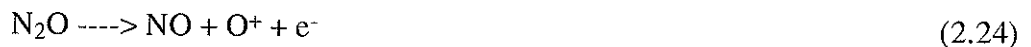
Photons with energies of 8-9 eV are able to create electron-hole pairs near the surface of the SiO<sub>2</sub> films. Holes may diffuse through the oxide and are trapped at the SiO<sub>2</sub>/Si interface. This may be why the damage is found mostly at the interface. Since the recombination of ions and electrons and the relaxation of excited neutral molecules may generate photons at some distance away from the plasma and as a result, the wafers which do not face the plasma may still be affected by photon radiation emitted by these radicals [13].

Because of the non-equilibrium between the gas molecules and the electrons, the electron temperature may reach 10<sup>4</sup> K while the gas temperature remains at 300 K. Certain reactions can be carried out inside the plasma at relatively low gas temperatures

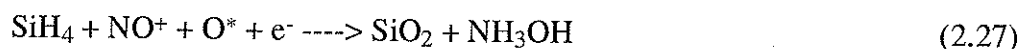
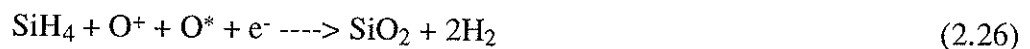
because most of the energy required by the reactions in the plasma is provided by electrons excited to very high states.

Figure 2.2 (a) and (b) show the differences between the thermal oxidation process and the PECVD process, respectively for the fabrication of  $\text{SiO}_2$  films. In the conventional thermal oxidation process, oxygen molecules from the gas ambient diffuse through the oxide layer to the  $\text{SiO}_2/\text{Si}$  interface and react with the silicon atoms there to form  $\text{SiO}_2$  films. Silicon atoms are supplied from the silicon substrate and consumed at the interface. In contrast, silicon atoms are supplied from the silane gas in the PECVD process. The silane reacts with the activated oxygen atoms or ions, which are formed from the dissociation of  $\text{N}_2\text{O}$  gas in the plasma to form  $\text{SiO}_2$  and  $\text{H}_2\text{O}$ . Silicon dioxide is then deposited layer by layer onto the silicon substrate and the water vapor is pumped out of the system.

$\text{N}_2\text{O}$  molecules are dissociated by the microwave radiation into a variety of ions, atoms, and electrons such as  $\text{NO}^+$ ,  $\text{O}^*$ ,  $\text{O}^+$ , and  $e^-$ . The activated  $\text{O}^*$  atoms and  $\text{O}^+$  are highly reactive and these species are the fundamental elements to react with silane to produce silicon dioxide molecules. The dissociation of  $\text{N}_2\text{O}$  can be described as follows:



The dissociation species of  $\text{N}_2\text{O}$  then react with silane:



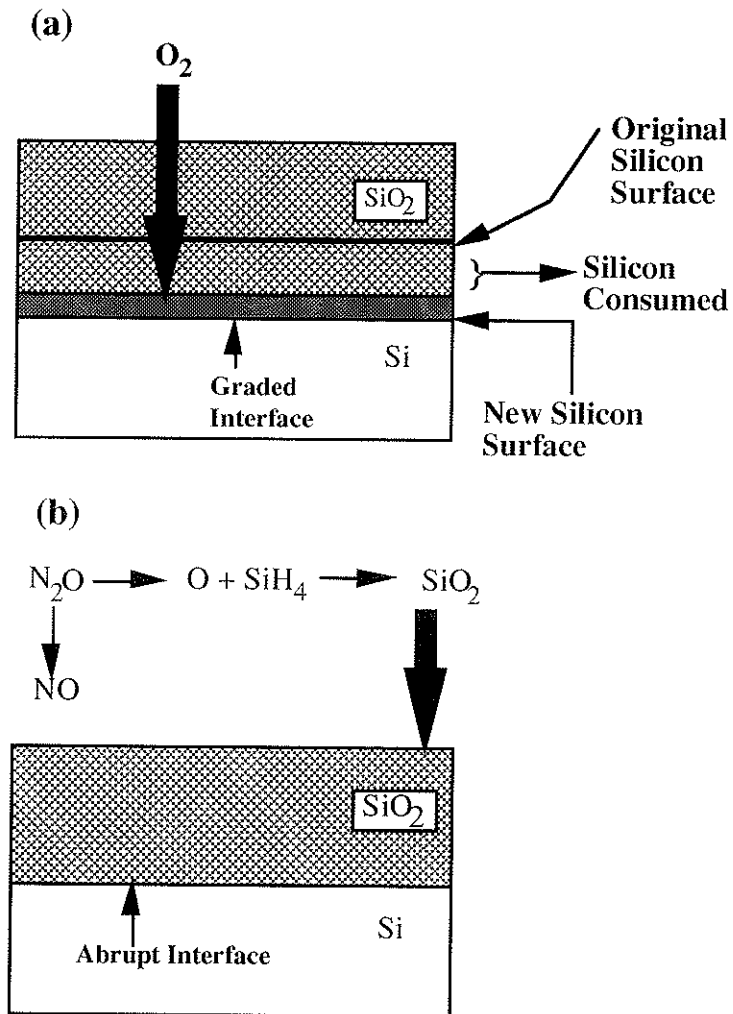


Figure 2.2 (a) Schematic diagram showing the thermal oxidation process for the fabrication of the SiO<sub>2</sub> films, and (b) Schematic diagram showing the PECVD process for fabrication of the SiO<sub>2</sub> films.

## 2.4 The Plasma Processing System and Species Selector and Energy Controller (SSEC)

The plasma chamber and processing chamber are constructed as a stainless steel waveguide, 34 cm long with standard dimensions of the WR-284 waveguide. The ECR microwave system used in this research to produce the SiO<sub>2</sub> films is shown in Fig. 2.3.

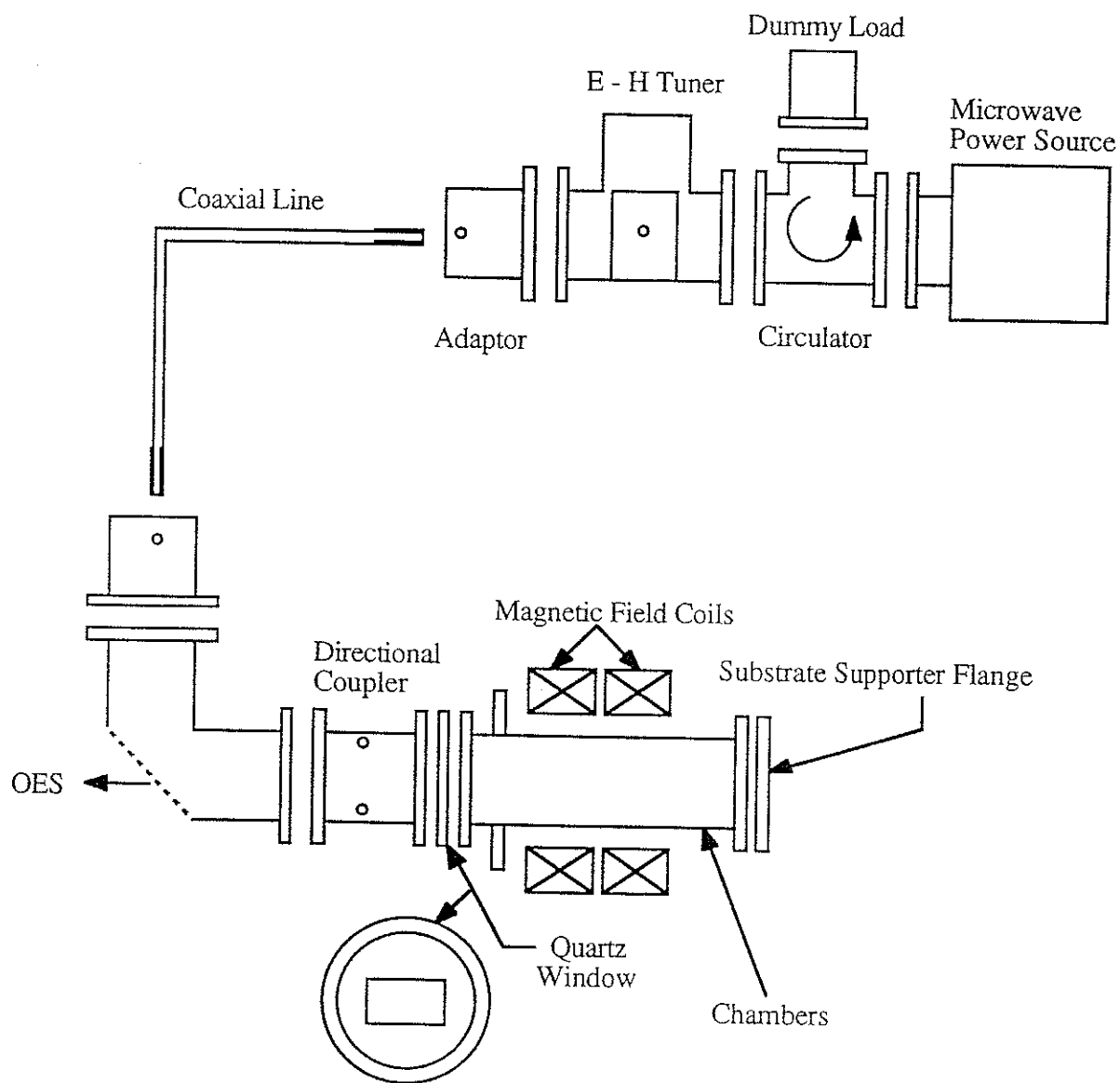


Figure 2.3 The ECR microwave plasma system.

A turbomolecular pump is used in conjunction with a chemical rotary pump for evacuating the system to a base pressure of  $10^{-6}$  Torr. A water-cooled coil is mounted around the plasma chamber to provide an axial magnetic field for confining the plasma in the transverse direction and creating an the ECR condition. The end of the plasma chamber is vacuum-sealed by a quartz window, which is used for sampling the plasma by the optical emission spectroscopy (OES) and microwave power feeding. The end of the processing chamber is held by a stainless steel substrate supporter flange. The microwave power is fed through the quartz window in the  $TE_{10}$  mode. The plasma chamber and the processing chamber can be heated to any temperature up to  $400^{\circ}\text{C}$  by a thermostatically controlled heating element surrounding the chambers. The plasma is characterized by optical emission spectroscopy (OES). The emission from the plasma is sampled through a quartz window. The emitting light on a  $25\ \mu\text{m}$  slit of a Jarrell-Ash Monospec 27 spectrometer is focused by a set of quartz lenses and mirrors. The Jarrell-Ash Monospec 27 spectrometer is equipped with a 1200 groove/mm grating and 1024 diode array EGG-PARC multichannel analyzer. The OES is taken at the chamber operating pressure, which is in the range of  $10^{-1}$  to  $10^{-3}$  Torr. The OES spectrum shows the intensities of different species in the plasma.

The apparatus of 'species selector and energy controller (SSEC)' is located between the plasma chamber and the processing chamber. Its function is to suppress the traffic of the energetic electrons, ions, and photons in order to avoid their bombardment on the substrates and the on-growing films. Under the ECR condition, the plasma chamber contains a mixture of ions, electrons, neutral atoms and molecules, activated atoms and molecules, oxidizing species, and photons of various energies. The SSEC acts as a filter to filtrate out the charged particles and photons. Figure 2.4 shows the schematic diagram of the plasma and processing chambers and the SSEC.

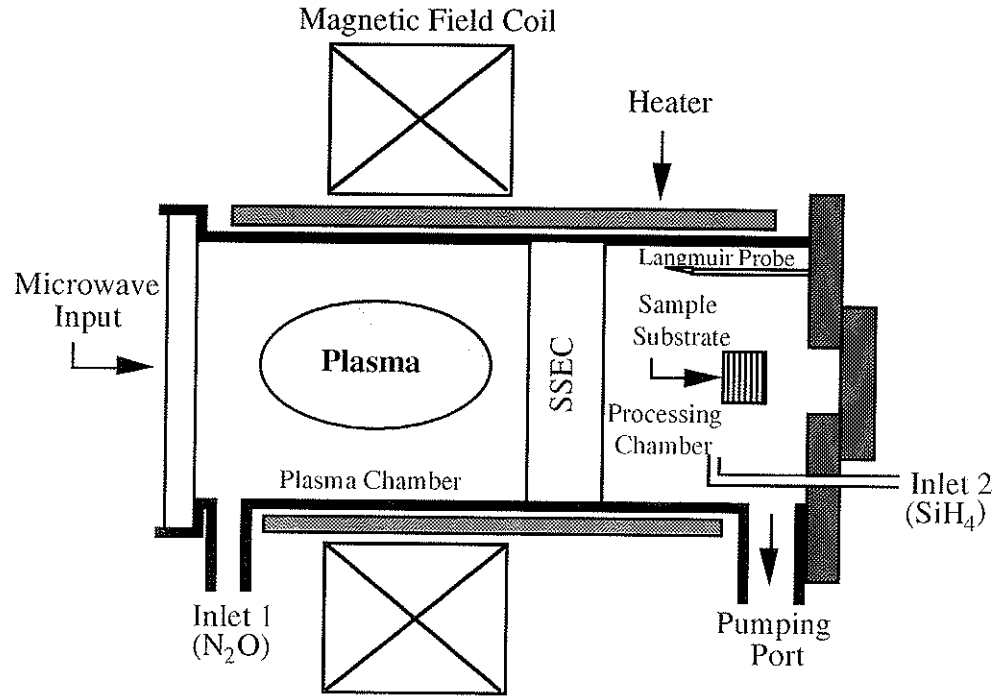


Figure 2.4 Schematic diagram of the plasma and processing chambers and the position of the SSEC.

In the plasma the charged particles (ions and electrons) gain their energies from the input microwave power. The charged particles after passing through the SSEC will not regain their energy because the microwave is reflected by the SSEC. The SSEC maintains a slightly higher pressure in the plasma chamber than that in the processing chamber thus preventing the upstream flow of  $\text{SiH}_4$  from entering the plasma chamber. This reduces the possibility of the formation of microdust particles.

## 2.5 $\text{SiO}_2$ Films Fabricated by ECR Microwave Plasma

The basic difference between the ECR microwave PECVD and the thermal oxides is that the thermally grown oxide is formed by the diffusion of oxygen species through  $\text{SiO}_2$  to the  $\text{SiO}_2/\text{Si}$  interface, while the ECR microwave PECVD oxide is formed layer by layer on the silicon surface. Therefore, in the case of the PECVD oxide films, the silicon substrates must have a contaminant-free surface condition because the original silicon surface, which later becomes the  $\text{SiO}_2/\text{Si}$  interface is likely to contain more

contaminants from the environment. In addition, the  $\text{SiO}_2/\text{Si}$  interface of the PECVD oxide films is believed to have a higher density of dangling bonds because of the incompatibility between the silicon substrate lattice and the silicon oxide lattice. Both of the contaminants and the dangling bonds create charges and defects at the  $\text{SiO}_2/\text{Si}$  interface, resulting in a high interface trap density, and hence affecting the threshold voltage and the surface carrier mobility of the MOS device. As a result, the feasibility of the PECVD oxide to be used as gate oxide depends greatly on the degree of contaminants on the surface of the silicon substrates prior to deposition.

Another vital factor to control the properties of the PECVD  $\text{SiO}_2$  films is the source gases. It should be noted that a source gas for a given element to be incorporated into a PECVD  $\text{SiO}_2$  film needs to be a gaseous or a volatile compound of that element. If a mixture of source gases is to be used, as is usually the case, the combination must be chosen that the composition gases do not react in the absence of a plasma, otherwise, gas-phase reaction will occur in the mixing manifold, giving rise to unwanted incorporation and pinholes in the deposited film. The inert gases (e.g., Ar, Ne or He) or reducing gases (e.g.,  $\text{H}_2$ ) are frequently used as diluents or carrier gases. Source gases may be obtained pure, or diluted in compressed gas cylinders. The usual source gases for  $\text{SiO}_2$  deposition are  $\text{SiH}_4$  and  $\text{N}_2\text{O}$ , often with  $\text{SiH}_4$  diluted in an inert gas such as Ar. Other source gas combinations which can be employed are  $\text{SiCl}_4/\text{O}_2$  and  $\text{Si}(\text{OC}_2\text{H}_5)_4/\text{O}_2$ . The most obvious combination of  $\text{SiH}_4$  and  $\text{O}_2$  cannot be used because these gases will react spontaneously on mixing (in the absence of plasma) to form  $\text{SiO}_2$  'smoke' in the gas phase.  $\text{N}_2\text{O}$  is chosen as the source of 'O' since it dissociates readily in a plasma, even though rather less readily than does  $\text{SiH}_4$ . Therefore,  $\text{N}_2\text{O}/\text{SiH}_4$  flow ratios appreciably in excess of 2 are needed to deposit PECVD  $\text{SiO}_2$  films. However,  $\text{N}_2\text{O}$  is more easily dissociated than  $\text{CO}_2$ , another possible 'O' source, where  $\text{CO}_2/\text{SiH}_4$  gas flow is around 200:1.

The quality of deposited  $\text{SiO}_2$  films depends strongly on the substrate temperature during deposition. For substrate temperatures between 175 and 200°C [46],

the films show a large discontinuous change. Below 175°C, the films are non-uniform, have a low density and refractive index, and a higher stress. Thus the films deposited below 200°C are not useful for applications.

The refractive index of the PECVD SiO<sub>2</sub> films is mainly determined by the Si/O stoichiometry (0.50-0.55) which is a function of the N<sub>2</sub>O/SiH<sub>4</sub> gas flow ratio. Above a N<sub>2</sub>O/SiH<sub>4</sub> flow ratio of 15 to 20 (for a deposition temperature of 200°C or above), the refractive index remains constant at 1.47, which is slightly higher than that of thermally grown SiO<sub>2</sub> films (1.464) and is probably due to a very slightly oxygen deficiency (< 2%). The small amount of oxygen deficiency may be due to the presence of some Si-H and Si-OH bondings in the films. The density of PECVD SiO<sub>2</sub> films (~ 2.30 gm cm<sup>-3</sup>) is slightly higher than that of thermal SiO<sub>2</sub> films (2.20 gm cm<sup>-3</sup>) [47].

## **2.6 Thermal Annealing**

Thermal annealing is a commonly used technique to reduce the amount of defects and associated traps formed during the radiation of MOS devices. The exact mechanism is not clearly established but it is generally agreed that thermal energy is the key catalyst to promote and sustain the various reactions during annealing. There are two schools of thought about thermal annealing in a forming gas. The first school relates to the bond relaxation mechanism during annealing while the second school relates to the hydrogenation of defects.

### **2.6.1 Relaxation of Strained Bonds**

The thermal annealing model is based on the hypothesis that annealing tends to relieve the stress induced on the Si-O strained bonds at the SiO<sub>2</sub>/Si interface by a high temperature oxidation process [49]. These strained bonds located at the SiO<sub>2</sub>/Si interface are caused either by the lattice mismatch between the Si substrate and the SiO<sub>2</sub> film (intrinsic stress), or by the differences in the thermal expansion coefficients between the

two materials (extrinsic stress). As a result, the annealing action can reduce the defects and related traps located at this strained region near the  $\text{SiO}_2/\text{Si}$  interface through a thermal reorientation process [56]. This implies that it heals the strained bonds. The dislocation of the Si-O bonds at the  $\text{SiO}_2/\text{Si}$  interface region during oxidation or deposition make the Si-O bonds to stretch tightly to match the silicon lattice. Since the stress on these strained bonds is being applied either intrinsically or extrinsically, the distortion of the Si-O bonds appear throughout the interfacial region indiscriminately so as to match the silicon lattice. However, the strained Si-O bonds are relieved and rearranged after annealing because the heat treatment relaxes the stress on the  $\text{SiO}_2$  lattice network and the  $\text{SiO}_2/\text{Si}$  interfacial region through the thermal vibration of atoms. This thermal annealing process thus eliminates the bond distortions.

### 2.6.2 Hydrogenation of Defects

The second annealing mechanism relates to the diffusion of hydrogen species to the  $\text{SiO}_2/\text{Si}$  interface as a catalyst to activate the chemical reactions occurring there. There are some experimental facts that have puzzled investigators for many years, which are:

- (1) MOS devices with a polysilicon gate anneal much slower than those devices with an active metal gate, such as aluminium or magnesium.
- (2) The speed of annealing is dependent on the lateral geometry for polysilicon gate devices, but not for aluminium gate devices.
- (3) MOS devices with an active metal gate can anneal even without ambient hydrogen.
- (4) Annealing of bare oxide interfaces proceeds more rapidly in hydrogen than in nitrogen.

The above findings clearly indicate that hydrogen annealing in Al gate MOS devices is not a straight forward 'diffusion and reaction' process. Balk [55] has shown that atomic hydrogen is produced at the  $\text{Al}/\text{SiO}_2$  interface by aluminium reacting with traces of water and the reaction is as follows:



In most cases, the water is in the form of hydroxyl groups strongly bonded to the silicon atoms on the oxide surface and is always present at the Al-SiO<sub>2</sub> interface. The atomic hydrogen then diffuses to the SiO<sub>2</sub>/Si interface and reacts with the interface traps. This hydrogen transport mechanism is generally accepted because it can explain all the above puzzles:

- (a) Polysilicon does not react with OH to form hydrogen atoms and diffusion through the gate metal is a slow process.
- (b) Since hydrogen is formed internally, external diffusion parameters certainly have no influence on the annealing rate.
- (c) External hydrogen is not the major hydrogen source for devices with active metal gates.
- (d) Hydrogen is proved to be essential in interface trap annealing.

The arrival of the mobile hydrogen species enables the defects to be annihilated and restores the bonding network through the following processes:



where ' $\equiv$ ' denotes three back bonds with oxygen in the SiO<sub>2</sub> network and ' $\bullet$ ' denotes an unpaired electron. Processes (2.29) and (2.30) show that the silicon dangling bonds react with the hydrogen atom and the hydroxyl group to form the Si-H and Si-OH bonds, respectively. Process (2.31) shows that the reaction between the non-bridging oxygen hole center and the hydrogen atom produces Si-OH bond. These reactions imply that hydrogen species are the key ingredients to passivate the defects so that the resulting products become electrically inactive in the MOS devices.

The hydrogenation effects described above confirm the importance of thermal energy in the annealing process. Basically, thermal energy serves three main purposes:

- (a) It promotes the generation of active hydrogen species, most likely atomic hydrogen;
- (b) It enhances the diffusion of those hydrogen species; and
- (c) It drives the defect-reaction process.

As a result, with proper control of the annealing conditions such as the ambient and temperature, the electrically active defects can be passivated and deactivated after annealing.

## CHAPTER 3

# FLUORINE-INCORPORATED SILICON OXIDE FILMS FABRICATED BY ECR MICROWAVE PLASMAS

The ECR microwave plasma-enhanced CVD system consists of a plasma chamber and a processing chamber. This system was developed and built by the Materials and Devices Research Group at the *University of Manitoba* [26]. We used the same system for the fabrication of fluorine-incorporated silicon oxide films (SiOF films).

The silicon substrates were n-type, <100> oriented, 2-6  $\Omega$ -cm wafers. The silicon substrates were cleaned by the RCA method [38], which will be described in Appendix A. After that, the substrates were dipped in a solution of 1% HF and deionized water to remove the native oxide and contaminants originally present on the substrate surface. After this cleaning process, the substrates had only a few monolayers of oxide when exposed to air atmosphere for 30 minutes [37]. The deposition parameters used were as follows:

Magnetic field for the ECR condition :	875 G
Microwave input power :	6.2 W
Gases :	5% of SiH <sub>4</sub> in Ar + CF <sub>4</sub> + O <sub>2</sub>
Substrate temperature:	305°C
Deposition time:	20 minutes

The silicon substrates were loaded into the processing chamber and placed on the floor of the chamber. The pressure of the gas mixture in the chamber was between 12 mTorr to 20 mTorr for different gas flow ratios, which was monitored by a capacitance manometer. Table 3.1 shows the gas flow rates used for various experimental conditions.

Table 3.1 The gas flow rates used for fabrication of SiOF films.

Gas Flow Rate (sccm)			Remark
SiH <sub>4</sub>	O <sub>2</sub>	CF <sub>4</sub>	
1-8	20	1	The study of the effect of SiH <sub>4</sub> concentration
1	10-40	1	The study of the effect of O <sub>2</sub> concentration
1	10	1-10	The study of the effect of CF <sub>4</sub> concentration

The SiOF films were characterized using a Bomem-Michelson 100 FTIR spectrometer for the IR absorption spectra and a Gaertner L119 null ellipsometer with a helium-neon laser light source (wavelength of 6328 Å) for the refractive index ( $n$ ) and the film thickness ( $d$ ). The uncertainties in the values of  $n$  and  $d$  were at most  $\pm 0.004$  and  $\pm 5$  Å, respectively.

The SiOF films were also characterized by X-ray emission spectroscopy (XPS) using Model SSX-100 X-ray spectrometer equipped with a monochromatized Al K $_{\alpha}$  X-ray source. As we do not have these equipments, we asked the *Surface Science Laboratory* at the *University of Western Ontario* to obtain the results for our Laboratory. The XPS spectra were obtained with a 600  $\mu\text{m}$  spot size and a 150 eV pass energy. Depth profiling was carried out with a 4 kV Ar<sup>+</sup> ion beam rastered over a 2x2 mm area to give a sputtered rate of 10 nm/minute for the SiOF films.

### 3.1 Infrared Absorption Spectra

There are four parameters from the infrared absorption spectra which are generally used to characterize the films:

- (1) The full-width at the half maximum (FWHM) and the frequency (or the wavenumber) for the occurrence of the maximum absorption (absorption peak) for the Si-O-Si stretching bands are strongly influenced by the bonding character, stoichiometry, density, and porosity of the films;
- (2) The intensity of the absorption bands near  $3650\text{ cm}^{-1}$  and  $3400\text{ cm}^{-1}$  due to hydrogen-bonded hydroxyl groups and absorbed water are indicative of the quality of surface hydroxyl groups and porosity of the oxides;
- (3) The impurities other than hydroxyl groups or water can be determined by their characteristic absorption bands; and
- (4) The approximate film thickness can be determined by the interference fringes in the spectrum.

For  $\text{SiO}_2$  films, the absorption bands near  $450$ ,  $800$  and  $1070\text{ cm}^{-1}$  are associated with the SiO rocking, bending, and stretching vibration, respectively. For SiOF films, an absorption band at  $930\text{ cm}^{-1}$  for Si-F bonding appears. The shifts of band peaks can be caused by oxygen deficiency, intrinsic stress arising from the bond strain, and the film density change. The common bands of SiOF film are summarized in Table 3.2, and a typical spectrum of the SiOF films between  $400\text{ cm}^{-1}$  and  $1400\text{ cm}^{-1}$  is shown in Fig. 3.1. The absorption spectrum depends on the gas flow rate and we have studied this gas flow rate dependence.

Table 3.2 The identification of different absorption peaks in SiOF films.

Approximate Position (cm <sup>-1</sup> )	Identified as
465	Si-O rocking
800	Si-O bending
930	Si-F
950	SiOH [13]
1070	Si-O stretching
3330	absorbed water [34]
3400	OH radicals
3650	SiOH [30, 32]

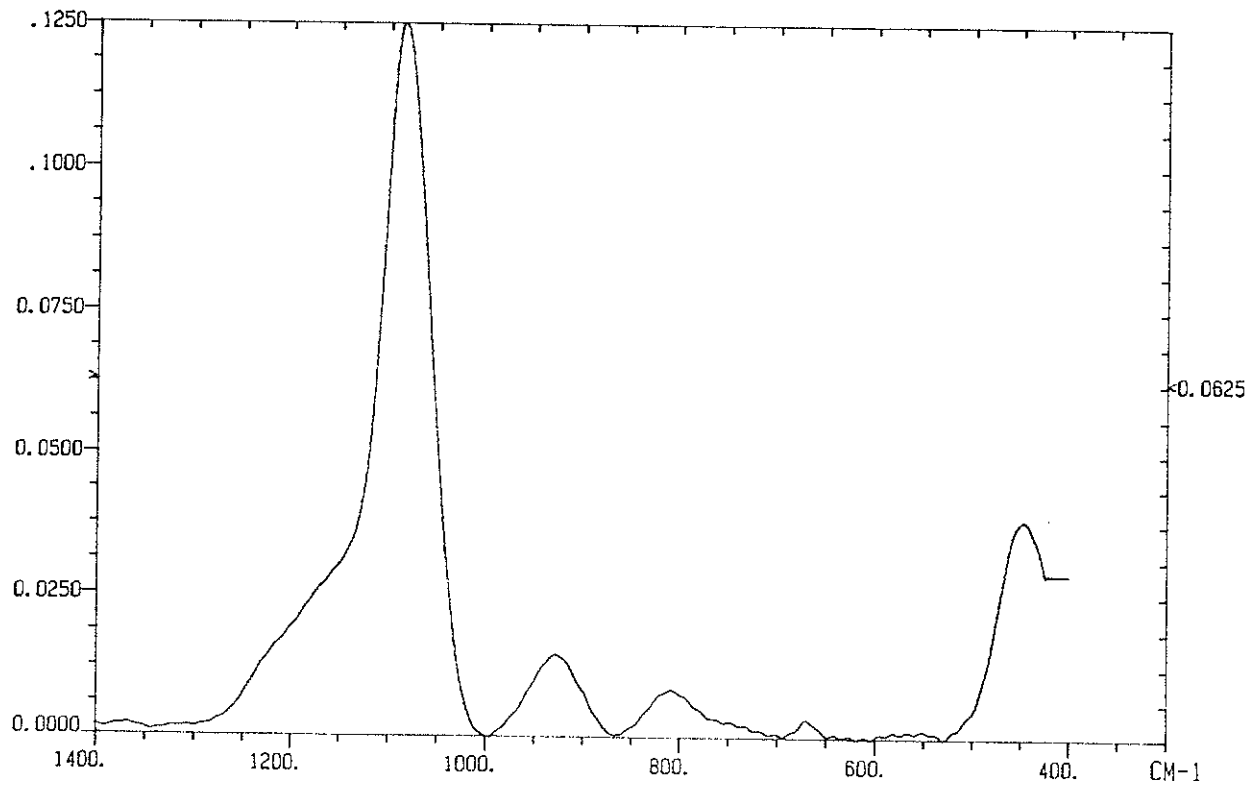


Figure 3.3 A typical FTIR spectrum of the SiOF films.

### 3.1.1 Dependence on the flow rate of CF<sub>4</sub> Gas

Figure 3.2 to 3.5 show the deposition rate, the refractive index, wavenumber for the SiO<sub>2</sub> stretching peak, the FWHM, and the SiF/Si-O-Si stretching absorption peak ratio as functions of the flow rate of CF<sub>4</sub> gas with the gas flow rates of oxygen and silane fixed at 10 sccm and 1 sccm, respectively. The gas flow rate of CF<sub>4</sub> which is raised from 0.05 sccm to 10 sccm corresponds to a change in pressure from 13 to 18 mTorr. It can be seen from Fig. 3.2 that the deposition rate increases with CF<sub>4</sub> concentration until it reaches 68 Å/min. After reaching the peak, it starts to decrease with increasing flow rate. The increase of deposition rate is associated with the stress relaxation effect [18]. The formation Si-F bonds in the SiOF films results in the breaking of the strained Si-O-Si ring since the Si-F bonds (bond energy ~5.37 eV) are much stronger than those of the Si-H and Si-OH weak bonds (bond energies in the range of 3 to 4 eV) in the non-fluorinated oxides. Also, fluorine has a higher electronegativity than those of oxygen and hydrogen. This mechanism tends to increase the number of fluorine atoms, which replace oxygen atoms, and also the number of Si dangling bonds. The oxygen atoms will react with silicon dangling bonds to form silicon oxides, and the fluorine atoms will be incorporated to form SiOF films. This action enhances the reactivity at the interface and subsequently the deposition rate of the SiOF films as the fluorine concentration is increased.

As the CF<sub>4</sub> flow rate is further increased, the replacement of oxygen by fluorine will increase. This implies that the oxygen becomes deficient for the fabrication of SiOF films. When the deposition rate reaches the peak, the concentration of oxygen and fluorine atoms are at the optimal level for the formation of SiOF films. Beyond this peak, the deposition rate will decrease because the number of fluorine atoms outnumbers that of oxygen atoms.

The refractive index of the SiOF films decreases exponentially with increasing flow rate of CF<sub>4</sub> gas and it is shown in Fig. 3.3. This implies that there is a change in the

composition of the film, such as the transformation of the film composition with the incorporation of  $\text{CF}_4$ . In general, the refractive index SiOF films is smaller than that of thermally grown  $\text{SiO}_2$  films (1.462). As the flow rate of  $\text{CF}_4$  gas is increased, more Si-O-Si rings are broken by fluorine. The formation of Si-F bonds opens up the oxide structure, thus inducing a relaxation of the interfacial strain. The refractive index is related to the dielectric constant (or permittivity) and hence the polarizability of the molecules inside the SiOF films. Therefore, the reduction in the refractive index also implies a reduction in dielectric constant and polarizability because of the reduction of the bond strain in the film.

Figure 3.4 shows the wavenumber  $\gamma_m$  for the occurrence of the Si-O-Si stretching absorption peak as a function of the flow rate of  $\text{CF}_4$ . The value of  $\gamma_m$  increases with increasing flow rate of  $\text{CF}_4$ . The value of  $\gamma_m$  is directly related to the intrinsic stress [33]. As the flow rate of  $\text{CF}_4$  gas is increased, the intrinsic stress decreases or in other words, the stress relaxation in the SiOF film increases, thus resulting in an increase in the value of  $\gamma_m$ . The substrate temperature during PECVD of SiOF films is relatively low ( $\sim 300^\circ\text{C}$ ) and the deposition rate is rather high. Therefore, the chance for the atoms to reach their lowest energy state and hence the most dense structure of the films is low, which resulting in the films with a porous structure and a high bond strain. However, as the flow rate of  $\text{CF}_4$  gas increases, more strained Si-O-Si rings are broken by fluorine to form Si-F bonds and this can offset the increase in bond strain due to the fast deposition rate. As a result, the SiOF films deposited at high  $\text{CF}_4$  gas flow rates have less bond strain.

Figure 3.5 shows that the FWHM decreases with increasing flow rate of  $\text{CF}_4$  gas and that the SiF/Si-O-Si absorption peak ratio increases linearly with increasing flow rate of  $\text{CF}_4$  gas. These two curves are consistent in that as  $\text{CF}_4$  concentration increases, the number of fluorine ions increases and therefore, more Si-O-Si strained bonds are broken by fluorine to form the Si-F bonds. The decrease of FWHM means the relief of the bond strain [35] which is consistent with the trend of  $\gamma_m$  shown in Fig. 3.4. It should be noted

that the rate of change of the refractive index, the wavenumber for the occurrence of the Si-O-Si stretching absorption peak and FWHM of the SiOF films start to decrease when the increase of the flow rate of  $\text{CF}_4$  gas is beyond 6 sccm. It is consistent with the results given in Fig. 3.2, in which the deposition rate of the SiOF films starts to decrease for the flow rate of  $\text{CF}_4$  gas higher than 6 sccm. Excess fluorine incorporation leads to the deficiency in oxygen. For the flow rate of  $\text{CF}_4$  gas larger than 6 sccm, the excess fluorine does not act to enhance the deposition rate, but instead to etch the SiOF films.

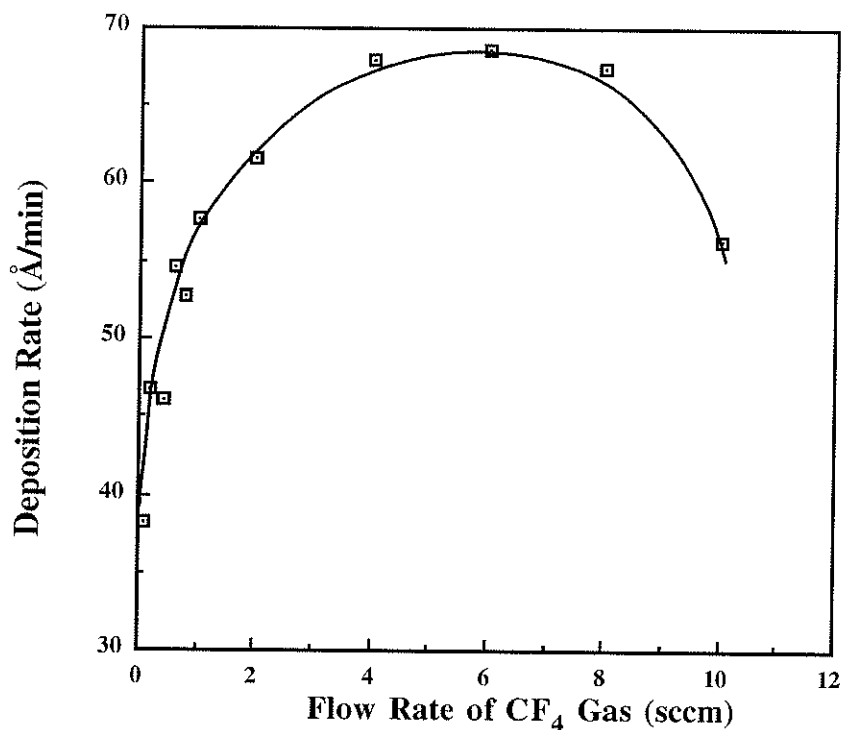


Figure 3.2 The deposition rate of the SiOF films as a function of the flow rate of  $\text{CF}_4$  gas with oxygen and silane gases at fixed flow rates of 10 and 1 sccm, respectively.

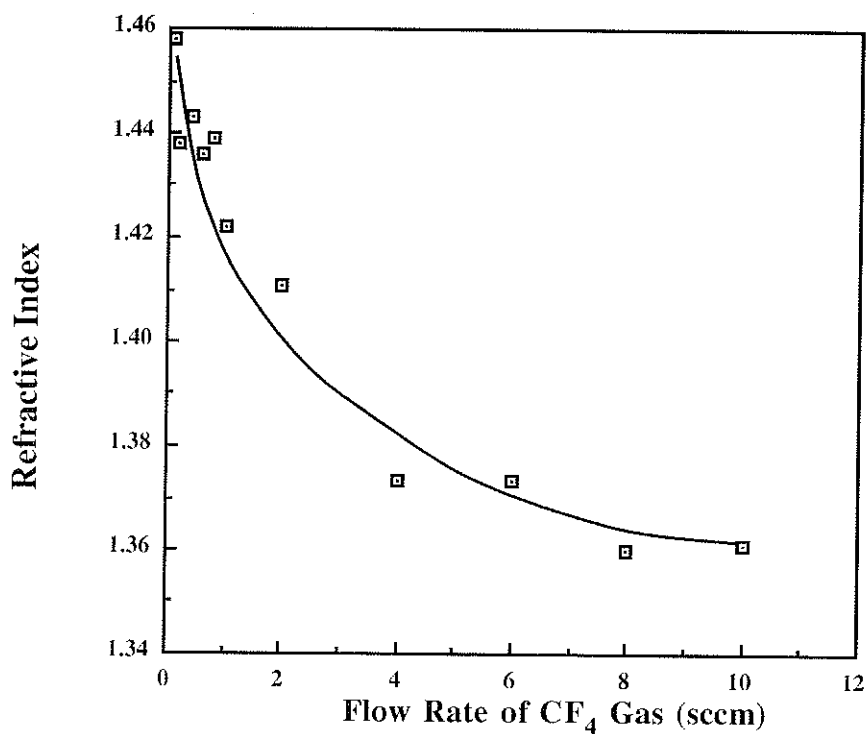


Figure 3.3 The refractive index of the SiOF films as a function of the flow rate of CF<sub>4</sub> gas with oxygen and silane gases at fixed flow rates of 10 and 1 sccm, respectively.

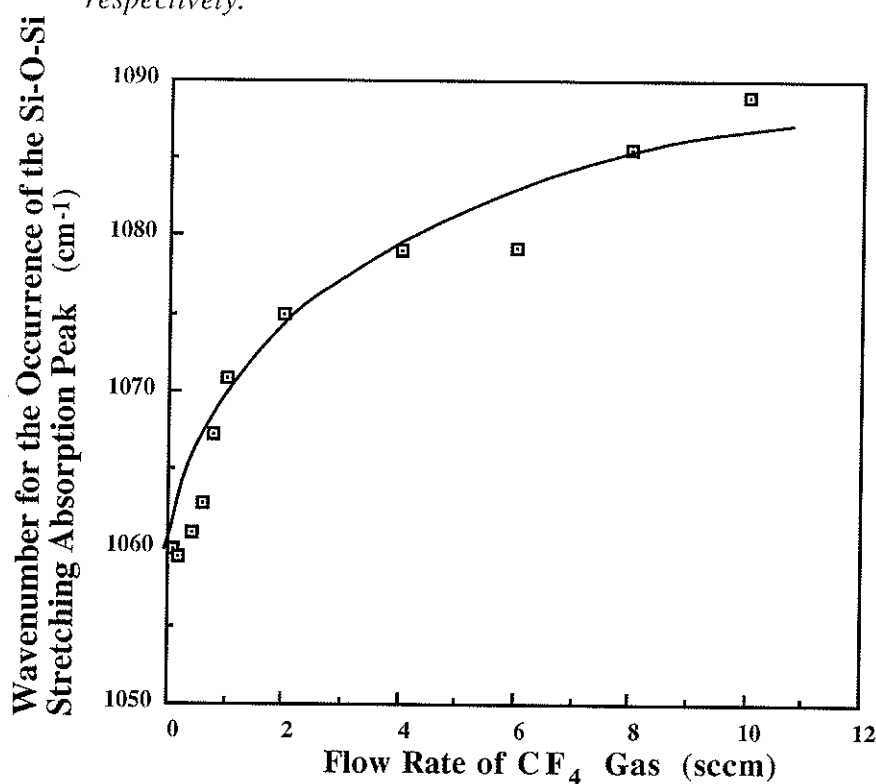


Figure 3.4 The wavenumber for the occurrence of the Si-O-Si stretching absorption peak of the SiOF films as a function of the flow rate for CF<sub>4</sub> gas with oxygen and silane gases at fixed flow rates of 10 and 1 sccm, respectively.

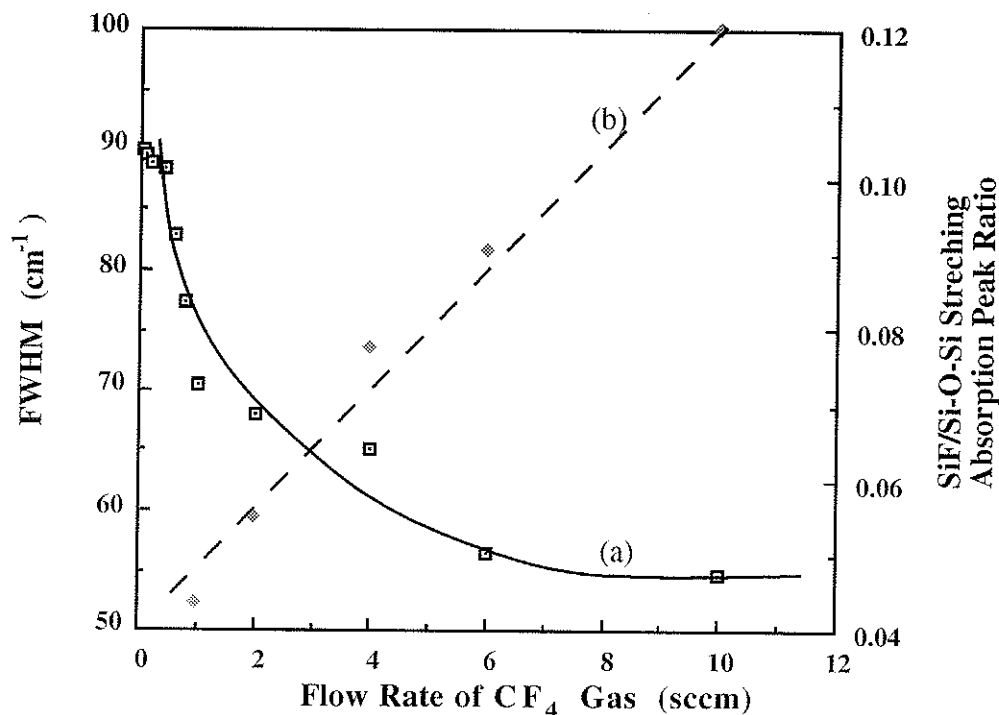


Figure 3.5 FWHM (a) and the SiF/Si-O-Si stretching absorption peak ratio (b) of the SiOF films as functions of the flow rate of CF<sub>4</sub> gas with oxygen and silane gases at fixed flow rates of 10 and 1 sccm, respectively.

### 3.1.2 Dependence on the Flow Rate of Oxygen Gas

In contrast with the dependence of the flow rate of CF<sub>4</sub> gas, the deposition rate, the wavenumber for the occurrence of the Si-O-Si stretching absorption peak, and the SiF/Si-O-Si absorption peak ratio decrease while refractive index increases with increasing flow rate of O<sub>2</sub> gas with the flow rates of CF<sub>4</sub> and silane kept constant at 1 sccm, as shown in Fig. 3.6-3.8. Since silane flow rate is kept constant, the deposition rate will be limited by the fixed amount of Si available. As the flow rate of oxygen is increased the excess oxygen ions will react with CF, CF<sub>2</sub>, and CF<sub>3</sub> to form CO and CO<sub>2</sub>, thus creating more fluorine atoms. The excess fluorine atoms will react with Si to form Si-F bonds, resulting in the decrease in deposition rate.

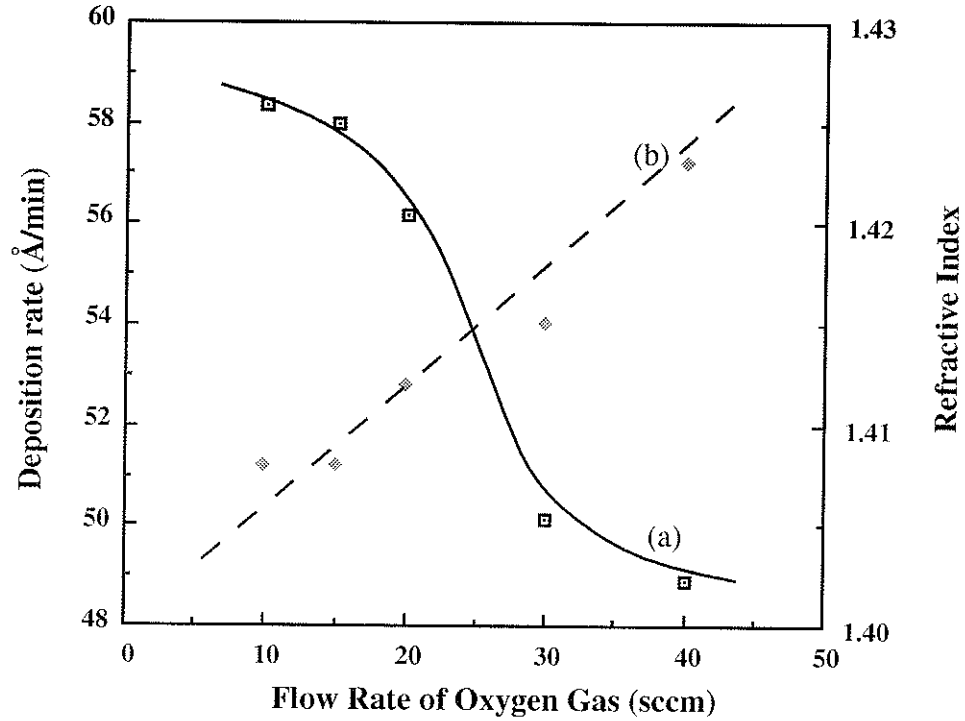


Figure 3.6 Deposition rate (a) and refractive index (b) of the SiOF films as functions of flow rate of oxygen gas with both silane and  $CF_4$  flow rates at 1 sccm.

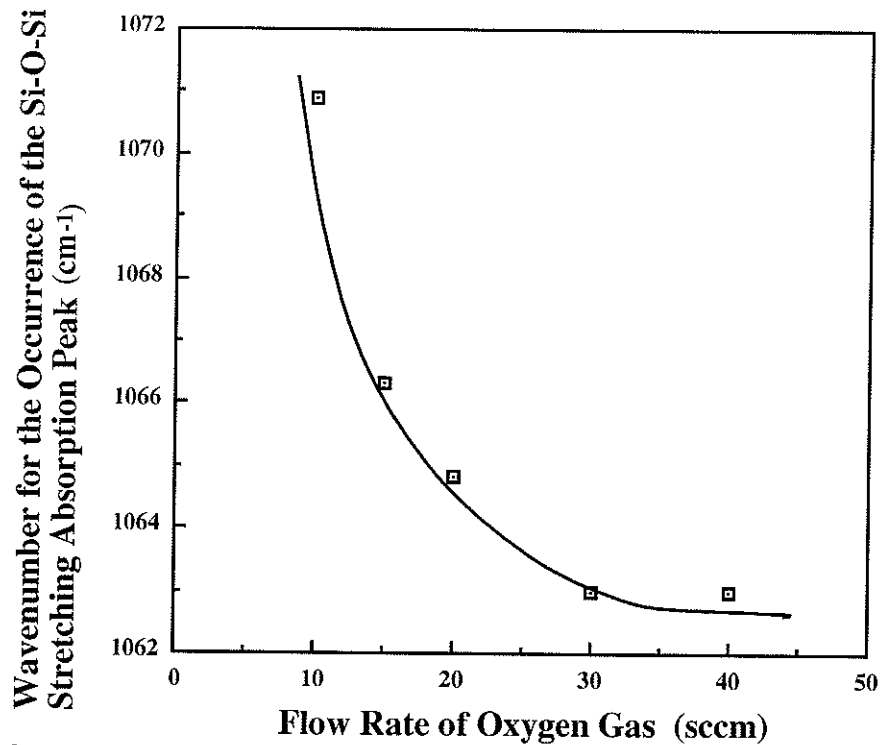


Figure 3.7 Wavenumber for the occurrence of the Si-O-Si stretching absorption peak of the SiOF films as a function of the flow rate of oxygen gas with both silane and  $CF_4$  flow rates at 1 sccm.

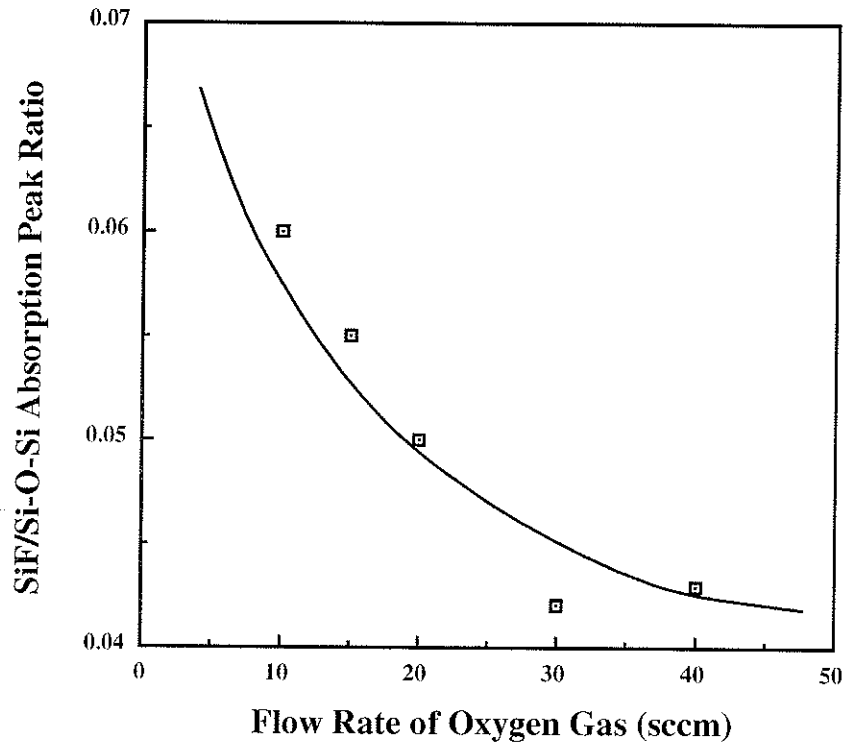


Figure 3.8 *SiF/Si-O-Si absorption peak ratio of the SiOF films as a function of the flow rate of oxygen gas with both silane and CF<sub>4</sub> flow rates at 1 sccm.*

In our experiments, as the flow rate ratio of oxygen/silane is larger than 10, there is no deficiency in oxygen. As the flow rate of oxygen gas is increased, the deposition rate of the SiOF films decreases, which is shown in Fig. 3.6, implying that the atoms in SiOF films have a better chance to assume their lowest energy state and to form a denser structure of the film. This is why the refractive index increases with increasing flow rate of oxygen gas because the film becomes less porous and less bond strain. In this case, the etching reaction of fluorine may be more dominant than the promotion of the formation of SiOF film. The etching reaction may be due to the following processes [44]:



which results in the formation of the gaseous  $\text{SiF}_4$  which is pumped out from the system. As a result, the Si-F bonds in the SiOF films subsequently decreases. It should be noted that the SiF/Si-O-Si absorption peak ratio decreases as the flow rate of oxygen gas increases beyond 25 sccm. This may due to the limit of the amount of fluorine atoms available for forming Si-F bonds.

### 3.1.3 Dependence of the flow rate of silane gas

It is quite obvious that the deposition rate and the refractive index increase while the value of  $\gamma_m$  and the SiF/Si-O-Si absorption peak ratio decrease with increasing flow rate of silane gas with the oxygen and  $\text{CF}_4$  gases kept constant at flow rates of 20 and 1 sccm, respectively, as shown in Fig. 3.9-3.11. However, if the silane to oxygen ratio is larger than 0.1 (ie., silane gas flow rate higher than 2), the SiOF films will suffer the deficiency in oxygen and become silicon rich, which, in turn, results in an increase of refractive index. The decrease of the value of  $\gamma_m$  with the increase of silane flow rate may be explained as due mainly to the deficiency in oxygen although the SiOF films may have a less stress and a higher density.

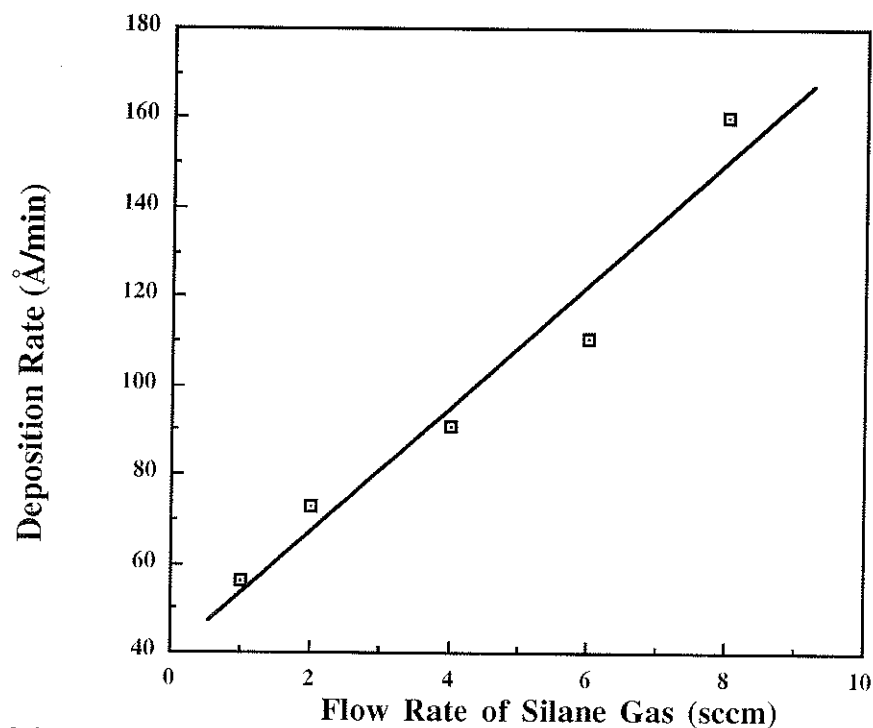


Figure 3.9 Deposition rate of the SiOF films as a function of the flow rate of silane gas with the oxygen and  $CF_4$  gases kept at constant flow rates of 20 and 1 sccm, respectively.

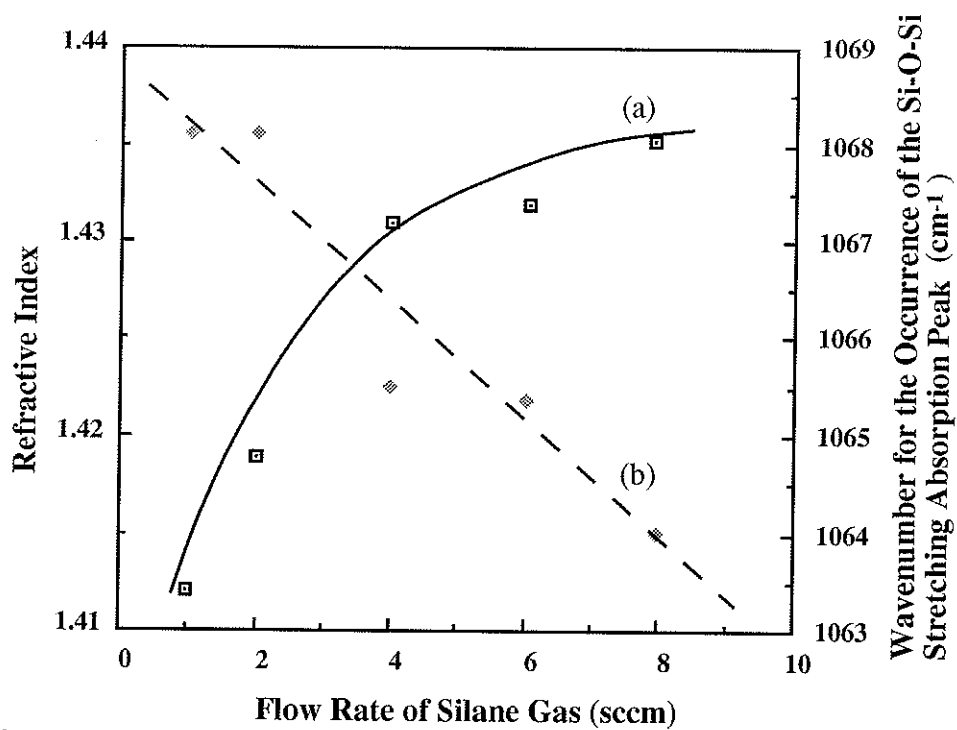


Figure 3.10 Refractive index (a) and wavenumber for the occurrence of the Si-O-Si stretching absorption peak (b) of the SiOF films as functions of the flow rate of silane gas with the oxygen and  $CF_4$  gases kept at constant flow rates of 20 and 1 sccm, respectively.

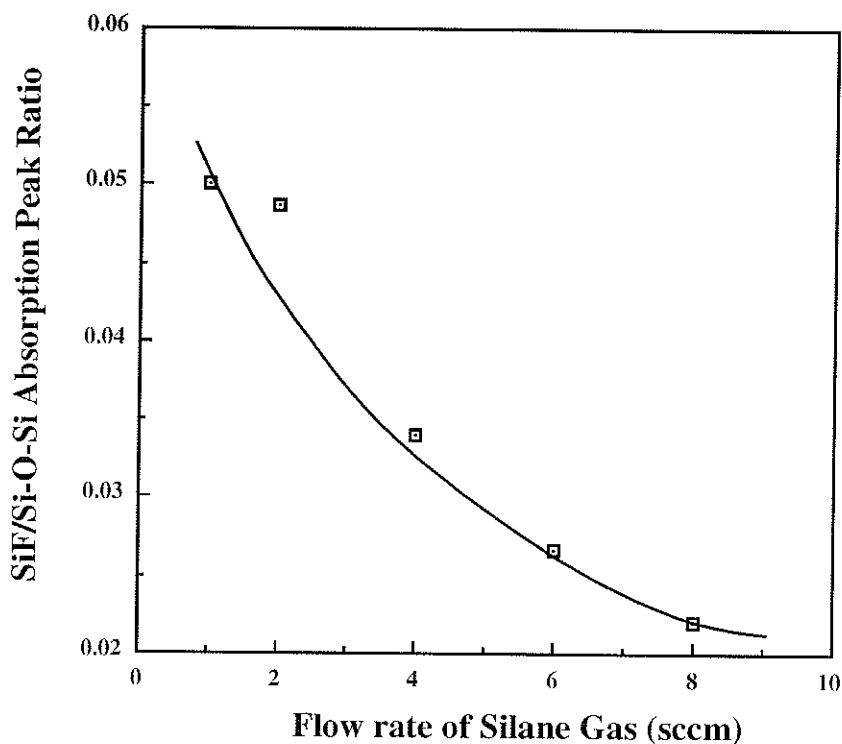


Figure 3.11 *SiF/Si-O-Si absorption peak ratio of the SiOF films as a function of the flow rate of silane gas with the oxygen and  $CF_4$  gases kept at constant flow rates of 20 and 1 sccm, respective.*

### 3.2 Heat Treatment of SiOF Films

Heat treatment is a commonly used technique for reducing the number of defects and associated traps formed during PECVD. One of the arguments, which has been well documented in the literature for the mechanism of heat treatment, is the bond relaxation mechanism. To study the effects of the heat treatment on the physical properties of the SiOF films, the samples of SiOF films without electrodes were heated at 400, 500 and 600°C in the nitrogen ambient for 30 minutes in a quartz tube. The heat treatment process began with nitrogen passing through a quartz tube in which the samples were placed for about 10 minutes in order to purge away any trace of dust and oxygen inside the tube. The samples were then placed on a quartz boat which was then inserted into the tube. The quartz boat was then pushed towards the hot zone of the quartz tube which had already heated to the desired heating temperature. After 30 minutes, the quartz boat was then

pulled out of the quartz tube and allowed to cool gradually to the room temperature. The cooling time was about 45 minutes. The SiF/Si-O-Si peak ratio and the wavenumber for the occurrence of Si-O-Si stretching peak were measured before and after heat treatment. We used three groups of samples for this investigation. These samples were produced using the gas mixtures described in Table 3.3:

*Table 3.3 The gas mixture used for fabrication of the SiOF samples for heat treatment experiments.*

Sample	Gas flow rate (sccm)		
	SiH <sub>4</sub>	O <sub>2</sub>	CF <sub>4</sub>
A	1	10	1
B	1	10	4
C	1	10	10

As the heat treatment temperature is increased, the SiF/Si-O-Si absorption peak ratio decreases as shown in Fig. 3.12. In pure SiO<sub>2</sub> films fabricated by ECR microwave plasmas, H<sub>2</sub> and H<sub>2</sub>O are the major gases annealed out from the sample during the heat treatment. In the case of the SiOF films, in addition to H<sub>2</sub> and H<sub>2</sub>O, a certain amount of fluorine atoms and HF gases might also be annealed out. Usami et al. [30] have reported that the atomic fluorine desorbs from the SiOF films at the heat treatment temperatures higher than 350°C. The desorption of atomic fluorine may be due to the dissociation of Si-F bonds. This is why the SiF/Si-O-Si absorption peak ratio decreases with increasing temperature. However, the effects of desorbed atomic fluorine on device reliability have not been clarified yet.

In general, heat treatment would induce stress relaxation, thus reducing bond strain in the SiOF films, which would, in turn, result in a higher Si-O-Si stretching frequency, as shown in Fig. 3.13. However, the result in Fig. 3.13 exhibits a reserve

trend. It is possible that the dissociation of fluorine species induces the formation of atomic fluorine and HF gas during the heat treatment. As a result, the amount of fluorine in the Si-F bonds decreases, and more Si-O-Si strained bonds may then be formed again. If this is the case, the increase of Si-O-Si strained bonds may offset the strain relaxation effect, leading to the decrease in the value of  $\gamma_m$  after heat treatment.

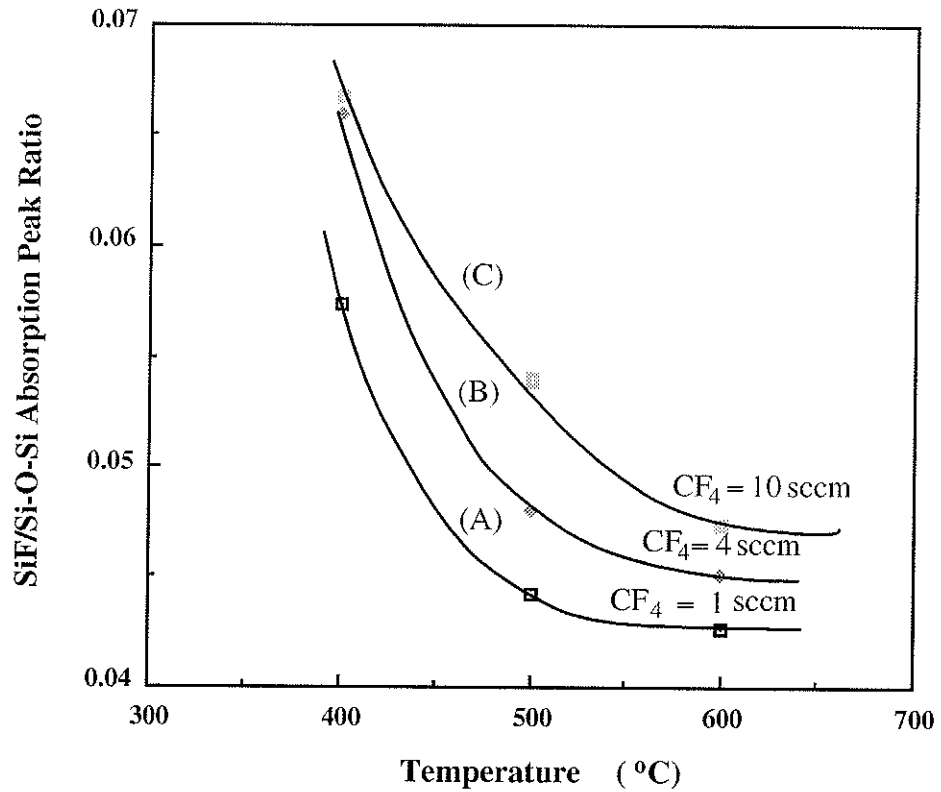


Figure 3.12 SiF/Si-O-Si absorption peak ratio as a function of heat treatment temperature for the SiOF samples (A)  $O_2$  : 10 sccm,  $SiH_4$  : 1 sccm  $CF_4$  : 1 sccm; (B)  $O_2$  : 10 sccm,  $SiH_4$  : 1 sccm  $CF_4$  : 4 sccm; (C)  $O_2$  : 10 sccm,  $SiH_4$  : 1 sccm  $CF_4$  : 10 sccm.

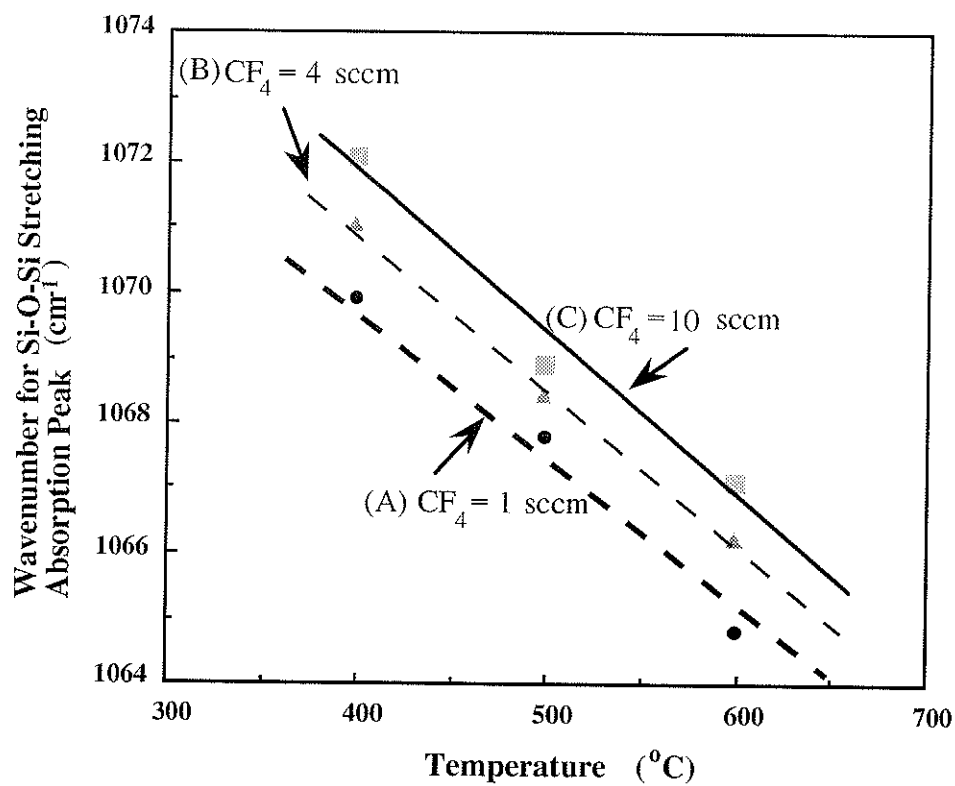


Figure 3.13 Wavenumber for the occurrence of Si-O-Si stretching absorption peak as a function of heat treatment temperature for the SiOF samples (A)  $O_2$ : 10 sccm,  $SiH_4$ : 1 sccm  $CF_4$ : 1 sccm; (B)  $O_2$ : 10 sccm,  $SiH_4$ : 1 sccm  $CF_4$ : 4 sccm; (C)  $O_2$ : 10 sccm,  $SiH_4$ : 1 sccm  $CF_4$ : 10 sccm.

### 3.3 X-Ray Photoelectron Spectroscopy (XPS)

X-ray photoelectron spectroscopy (XPS) is ideally suited for characterization of ultrathin oxide regions formed near a surface. The composition at the surface and subsurface of SiOF films can be determined from the analysis of XPS data. XPS can be used to obtain information on the most abundant surface atoms, with concentrations in the range of 0.01 monolayer or greater.

The chemical nature of Si, O, C and F bonds may be inferred by the magnitude and direction of the binding energy ( $E_B$ ) shift ( $\Delta eV$ ) for the core electrons of the atoms. The binding energy of an electronic level is given by:

$$E_B = h\nu - E_K - \phi \quad (3.3)$$

where  $h\nu$  is the energy of the x-ray excitation,  $E_K$  is the kinetic energy of the photoemitted electron as measured in the spectrometer, and  $\phi$  is a spectrometer constant. Binding energies are referenced to as the Fermi level. Changes in the chemical environment about an atom cause a binding energy shift. Core electron binding energy shifts have been correlated with electronegativities for a large number of compounds [38]. Some uncertainty exists in the relationship between core binding energies and chemical composition since both relaxation processes and changes in Fermi level also alter binding energies.

As we can see in the XPS spectra shown in Fig. 3.14, fluorine was easily detected by XPS. These spectra were obtained prior to any depth profiling and thus represent the surface chemistry of the outer  $\sim 50 \text{ \AA}$ . The composition data are summarized in Table 3.4. Additional work has also been carried out to characterize the 'bulk' composition of the films. In order to obtain accurate 'bulk' composition data, multiplex spectra for Si (2p), O (1s), F (1s), and C (1s) were obtained at sputter times of 0, 20, 40 and 60 second intervals. These sputter times represent the depth of 0, 3, 6 and 9 nm.

Table 3.4 Composition in atomic % of the SiOF films fabricated at gas flow rates of  $CF_4$  :  $O_2$  :  $SiH_4 = 10 : 10 : 1$  sccm.

Depth (nm)	Elements Detected (atomic %)			
	Si	O	F	C
0	33	50	2.2	15
3	46	50	2.4	1.1
6	45	52	2.7	–
9	45	52	2.5	–

Table 3.4 lists the atomic composition of the SiOF films fabricated with gas mixture of  $CF_4$ ,  $O_2$ ,  $SiH_4$  at the flow rates of 10, 10 and 1 sccm, respectively. Fluorine concentration is about 2.5 atomic percent relative to the four elements surveyed in the outer 9 nm of the SiOF film. The atomic percentages of silicon and oxygen increase with increasing depth, and saturate at the depths deeper than 6 nm. The ratio of Si to O is 1 to 1.16 at the depth deeper than 6 nm. It should be noted that there is carbon at the outer surface and at a depth of 3 nm. At deeper depths, however, carbon concentration drops below the minimum detection limit ( $\sim 0.2$  atomic %). Carbon existence may be due to the remaining reaction byproducts. During the deposition of the SiOF films,  $CF_4$  is dissociated and form fluorine ions and carbon. Carbon atoms are supposed to bond with oxygen ions to form CO and  $CO_2$ . However, there still have some carbon bonding with silicon or hydrogen to form Si-C bonds and aliphatic hydrocarbons [39]. The carbon residue is normally reacted with fluorine to form gaseous CF,  $CF_2$  and  $CF_3$ . As the deposition process comes to the end, the carbon atoms which left on the outer surface of the SiOF films could not find fluorine or

even oxygen atoms to react with and as a result, they became deposited as contaminant on the surface of the SiOF film.

Figure 3.14 shows the spectra of the SiOF sample fabricated in a gas mixture of  $\text{CF}_4$ ,  $\text{O}_2$  and  $\text{SiH}_4$  at flow rates of 10, 10 and 1 sccm, respectively. The binding energies of Si, C, O and F shown in Fig. 3.19 are given in Table 3.5.

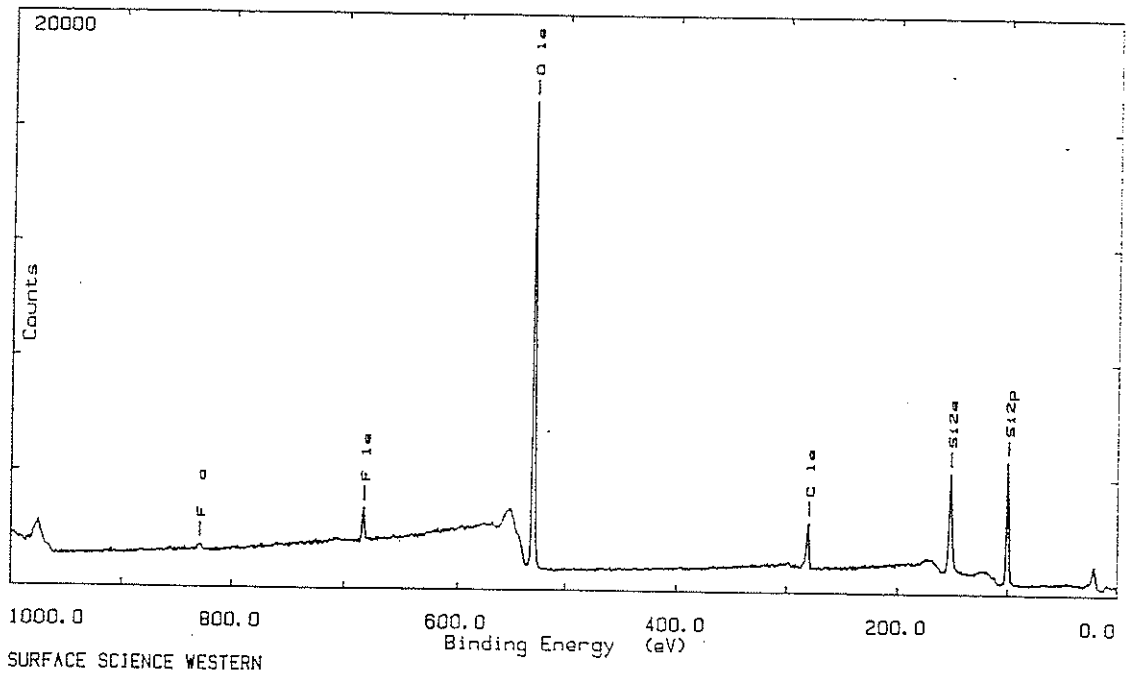


Figure 3.14 The XPS spectra of the SiOF film fabricated in a gas mixture of  $\text{CF}_4$ ,  $\text{O}_2$  and  $\text{SiH}_4$  at flow rates of 10, 10 and 1 sccm, respectively.

*Table 3.5 Binding energies of Si, C, O and F in SiOF films.*

Elements	Binding Energy (eV)
Si (2p)	101
C (1s)	282.4
O (1s)	532.3
F (1s)	685.8

For the Si (2p) peak, the 101 eV binding energy is due to the Si-F bonds [40]. This is consistent with the binding energy of fluorine (685.8 eV), which has been reported that this binding energy is due to the Si-F bonds [39]. The carbon binding energy is neither a high binding energy component suggestive of fluorine-carbon bonds (binding energy ~290 eV) [41] nor a low binding energy component suggestive of silicon-carbon bonds (binding energy ~283 eV) [40]. Therefore, the carbon signal probably originates from a physisorbed hydrocarbon layer not chemically bonded to silicon or carbon. As a result, the carbon detected by XPS shows that it plays little role in the electrical passivation of the surface. The presence of such hydrocarbon contamination which leads to the formation of surface silicon carbide can only be observed after high-temperature processing [43]. In addition, the peak position of Si (2p) shifts to a higher binding energy with increasing F (1s) peak intensity (i.e., increasing the amount of fluorine). As the amount of fluorine increases, more SiF<sub>2</sub> and SiF<sub>3</sub> bonds in the SiOF films are formed. The SiF<sub>2</sub> and SiF<sub>3</sub> bonds have binding energies of Si (2p) at 101.9 and 103.1 eV, respectively. Therefore, as the intensity of the F (1s) peak goes up, the binding energy of the Si (2p) will shift to a higher value.

## CHAPTER 4

# THE EFFECTS OF PHOTON RADIATION ON SiO<sub>2</sub> FILMS FABRICATED BY ECR MICROWAVE PECVD

The plasma-enhanced chemical vapor deposition (PECVD) technique is widely used for the fabrication of passivation layers for integrated circuits. One of the advantages of the PECVD processing is its low processing temperature, which is necessary for multilevel metallization routing. However, the quality of the deposited SiO<sub>2</sub> films are seriously affected by the bombardment of energetic ions, electrons, and photons produced in the plasma. It is still not clear whether the charged particles or the photons play the major role in the formation of various defects in the SiO<sub>2</sub> films. In order to study the effects of the charged particles and photon radiation on the properties of the deposited SiO<sub>2</sub> films separately, a charged particle suppressor has been designed to stop the bombardment of electrons and ions on the substrate and the on-growing films. In this chapter, we present our approach to this investigation.

### 4.1 Experimental Techniques and the Charged Particle Suppressor

The deposition system used in this study is the same as that described in Chapter 3. The major difference is that a charged particle suppressor instead of a SSEC was placed between the plasma chamber and the processing chamber.

The major function of the charged particle suppressor is to suppress the traffic of ions and electrons and it is placed at about the edge of the coil generating magnetic fields. The distance between the substrates and the charged particle suppressor is about 5 cm. The charged particle suppressor is made of stainless steel plate and consists of three

grids (stainless steel meshes), the separation between each other being 5 mm, as shown in Fig. 4.1. Each grid is isolated from each other and also from the chamber so that it can be biased with a positive or negative dc voltage. Ceramic coated aluminium wires and electric feedthrough are used to connect the charged particle suppressor to the external dc sources. The front grid faces the plasma volume while the back grid faces the substrate. The middle grid is connected to ground. The dc biasing can have three different modes depending on the polarity of the dc voltage at the front and the back grids. If one of the grids is biased with a negative voltage while the other biased with a positive voltage, the number of charged particles (ions and electrons) will be effectively suppressed from bombarding the substrates and the on-growing films. Since the charged particle suppressor is designed not to block the photon radiation, the effect of photon radiation on the  $\text{SiO}_2$  films during PECVD can be experimentally studied.

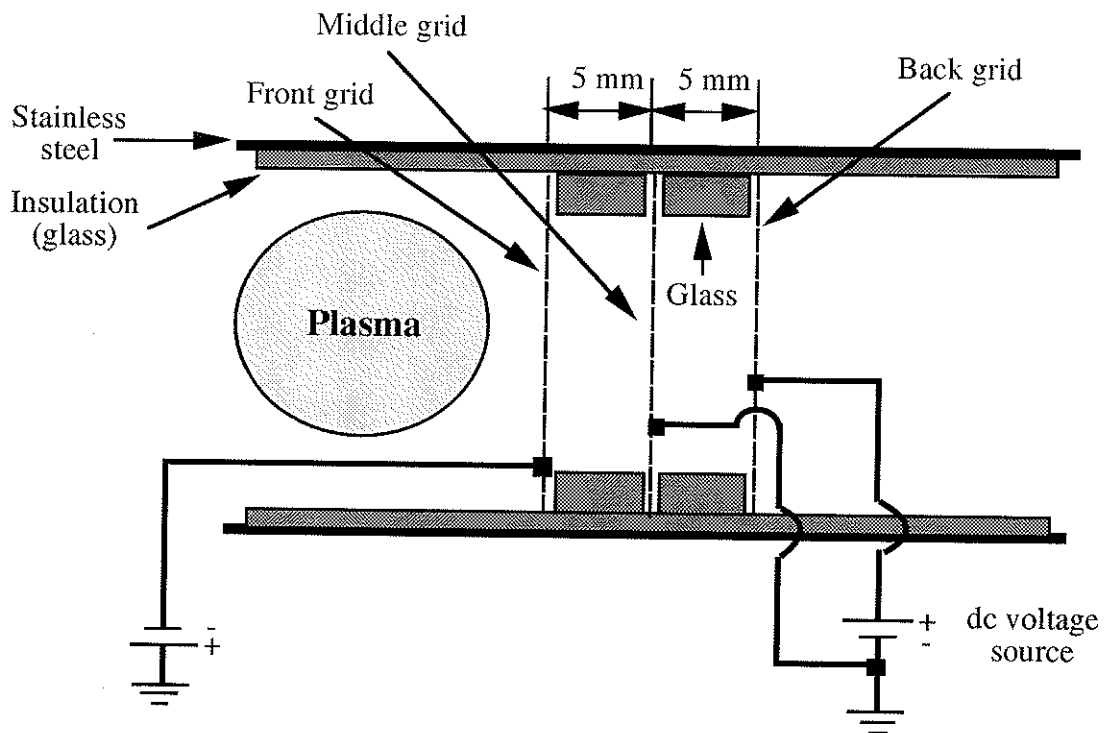


Figure 4.1 Schematic diagram of the charged particle suppressor.

By connecting the front and the back grids of the charged particle suppressor separately to two Hioki 3212 digital testers (potential meters) with the middle grid grounded, the floating potentials induced by the  $N_2O$  plasma have been measured. Using a tungsten Langmuir probe biased at +12 and -12 V and positioned at 5 cm behind the charged particle suppressor, we have also measured the electron and the ion currents from the  $N_2O$  plasma with a Keithley 610 C electrometer. It should be noted that the chamber walls must be grounded, otherwise a floating potential will be induced by the  $N_2O$  plasma on the chamber walls. The experimental arrangement for the measurements of the electron and the ion currents from the  $N_2O$  plasma is shown in Fig. 4.2.

The substrates were n-type,  $\langle 100 \rangle$  oriented, 2-6  $\Omega\text{cm}$  silicon wafers. The substrates were cleaned by the RCA method [38] (Appendix A). All  $SiO_2$  films were fabricated using the same deposition parameters as follows:

Magnetic field for the ECR condition :	875 G
Microwave input power :	6.2 W
Gases mixture flow rate: 5% of $SiH_4$ in Ar	: 1 sccm
$N_2O$	: 10 sccm
Substrate temperature:	305°C
Gas Pressure:	15 mTorr
Deposition time:	30 minutes

The external bias voltages applied to the grids varied from 25 to 40 for the back grid and -25 to -40 for the front grid. The Si substrates were divided into two groups, one was placed on the chamber floor horizontally to the chamber axis, which had almost no photon radiation. The other was held on a substrate holder which was mounted in such a way that the substrate surfaces were perpendicular to the chamber axis and directly exposed to the photon radiation. The substrate holder could also be heated to any temperature up to 400°C by a thermostatically controlled tungsten lamp inserted beneath the table surface. Comparing between the results of these two groups, the photon radiation effects can be estimated since

the external bias can suppress most of the electrons and ions and significantly reduce the amount of ion bombardment.

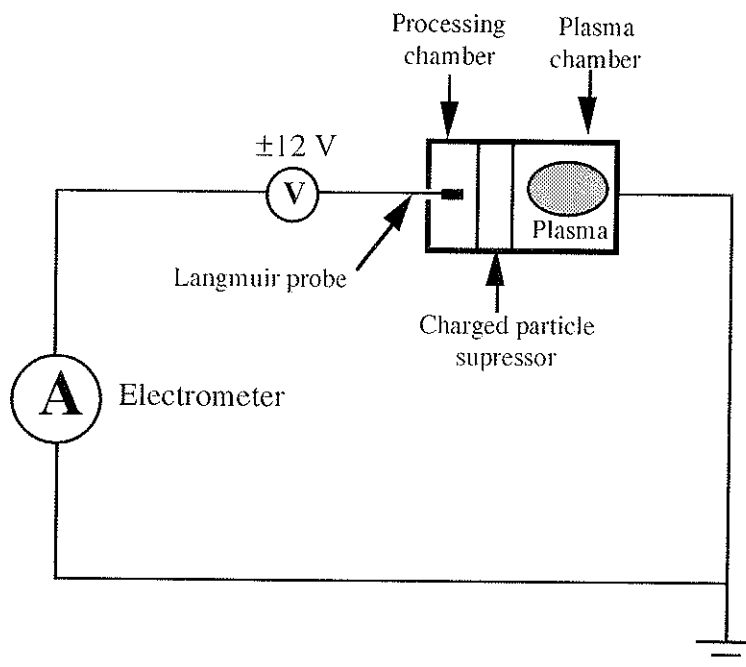


Figure 4.2 Experimental arrangement for the measurements of ion and electron currents from the  $N_2O$  plasma.

After the  $SiO_2$  films were deposited on Si substrates, the samples were immediately loaded into another vacuum system for metallization. The fabrication of MOS devices follows two steps:

- (1) The deposition of aluminium on the top of the  $SiO_2$  through the shadow mask to form the gate electrodes.
- (2) The deposition of aluminium on the silicon side to form the back electrode.

The size of each gate electrodes was  $5 \times 10^{-3} \text{ cm}^2$ . The aluminium films were thermally evaporated under a vacuum of  $10^{-6}$  Torr. The thickness of both the back contacts and gate electrodes was about  $1000 \text{ \AA}$ .

After metallization and the PMA treatment in a forming gas (10% H<sub>2</sub> in N<sub>2</sub>) at 400°C for 30 minutes, the SiO<sub>2</sub> films were characterized by high-frequency (1 MHz) C-V and quasi-static C-V measurements. For quasi-static C-V measurement a Hewlett Packard 4140B PA meter/dc voltage source was used as a linear voltage ramp, while for high-frequency C-V a Boonton 72AD capacitance meter was used in conjunction with a HP 4140B PA meter/dc voltage source. All measurements were performed at room temperature.

## 4.2 Floating Potential

The potential at the front grid at a constant gas flow rate of 10 sccm of N<sub>2</sub>O is negative with respect to ground because the sheath potential is built up on the surface of any object which is in contact with the plasma volume. When the positive ions pass through the charged particle suppressor, they may collide with the middle and the back grids. This causes a positive charge built up on this two grids. The total internal potential difference between the front and the back grids is about 6 V at the chamber pressure of 10 mTorr, which is shown in Fig. 4.3. The potential difference between the front and the back grids decreases with increasing gas pressure since the mean free path of the charged particles in the plasma decreases. Therefore the probability of particle collision increases which then reduces the life time of the charged particles. For most ECR microwave PECVD operations, the gas pressure used is between 10-20 mTorr. Within this range, the potential difference between the front and back grids is about 3.5-4.5 V. In addition, the floating potential measured by the tungsten Langmuir probe at a point 5 cm from the back wall is 6.5 mV negative with respect to ground. This means that there is a certain number of electrons entering the processing chamber.

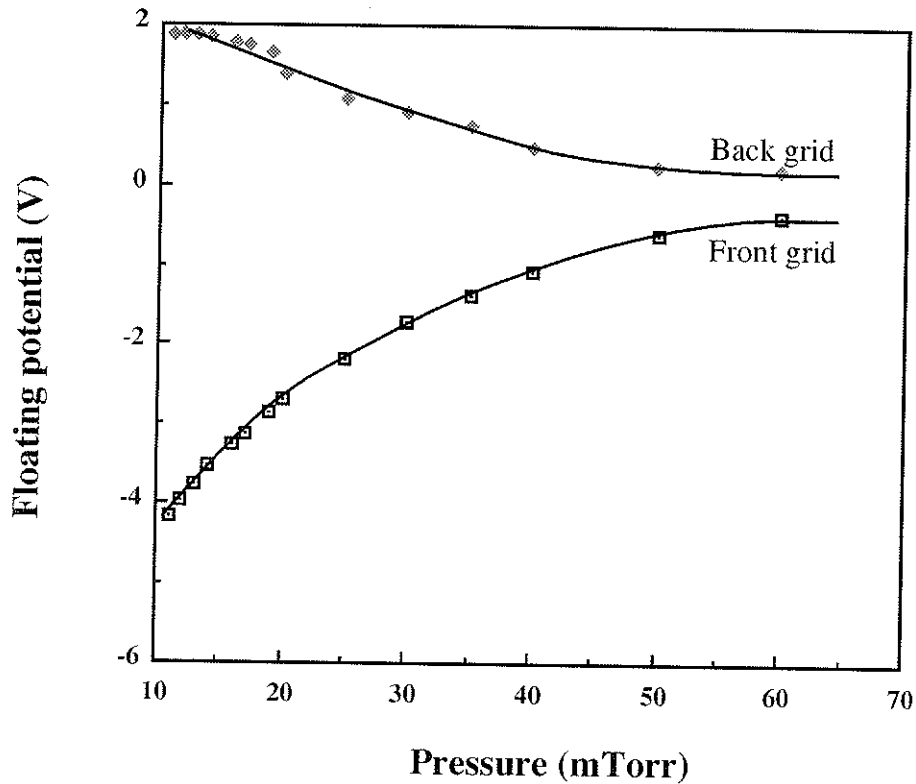


Figure 4.3 The floating potentials induced by the  $N_2O$  plasma (10 sccm) at the front and the back grids.

### 4.3 Ion and Electron Currents

Without biasing the charged particle suppressor, the electron and ion currents are in the order of  $10^{-7}$  A. In order to suppress the number of positive ions and electrons passing through the charged particle suppressor and flowing toward the substrates, the front grid was negatively biased while the back grid was positively biased. This bias arrangement is the most efficient way to reduce both the electrons and the ions flowing toward the substrates. The negatively biased front grid tends to attract positive ions toward it and to repel the electrons. When the ions enter the charged particle suppressor, the electric field in the region between the front grid and the central ground grid tends to block them to pass through the middle screen. However, some of the ions and electrons may still go through to reach the back grid. Even electrons can pass through the negatively biased front grid and the middle grid, it is difficult for them to travel far away from the back grid,

which is positively biased. The positively biased back grid can also repel positive ions from entering the processing chamber.

It should be noted that the currents measured by the tungsten Langmuir probe may also be due to the photoionization by the photon radiation. In order to define the range of the external bias voltage which can suppress effectively the traffic of ions and electrons, 5 biasing arrangements were used as given in Table 4.1. The flow rate of  $N_2O$  was 10 sccm and the gas pressures used were from 10 to 70 mTorr. The results for the biasing arrangements A, B and E are shown in Fig. 4.4-4.6. It should be noted that the biasing arrangements C to E, which are biased at  $\pm 30$ ,  $\pm 35$  and  $\pm 40$ , respectively, give almost identical electron and ion currents.

*Table 4.1 The biasing arrangements for the measurements of electron and ion currents induced by the  $N_2O$  plasma.*

Biasing arrangement	Bias Voltages (V)	
	Front screen	Back screen
A	0	0
B	25	-25
C	30	-30
D	35	-35
E	40	-40

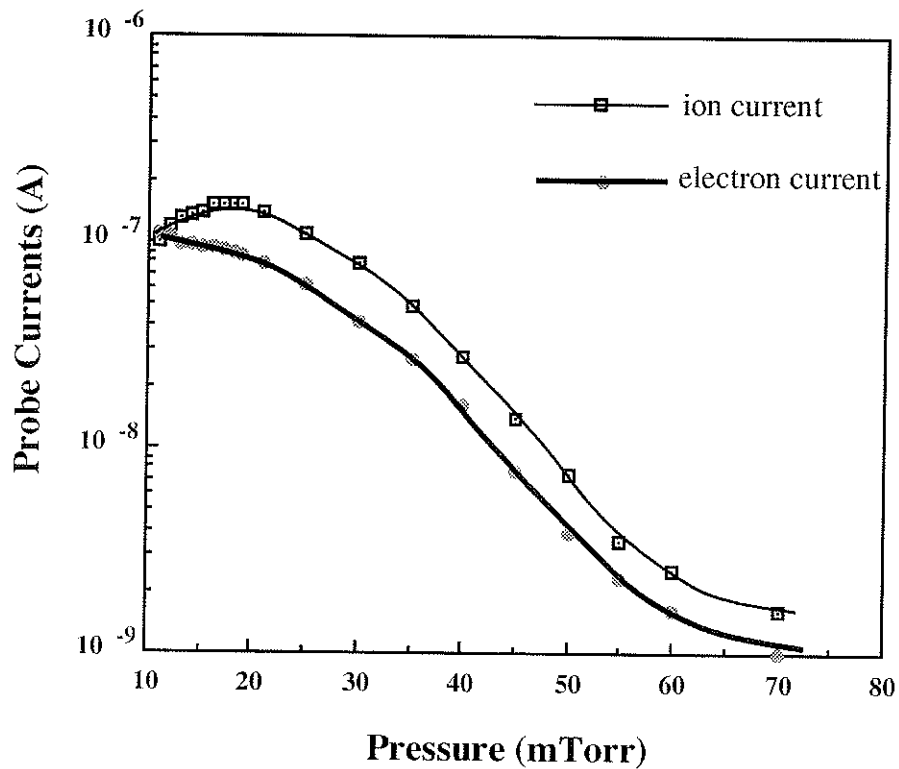


Figure 4.4 Ion and electron currents of the  $N_2O$  plasma as functions of pressure without external bias (Arrangement A).

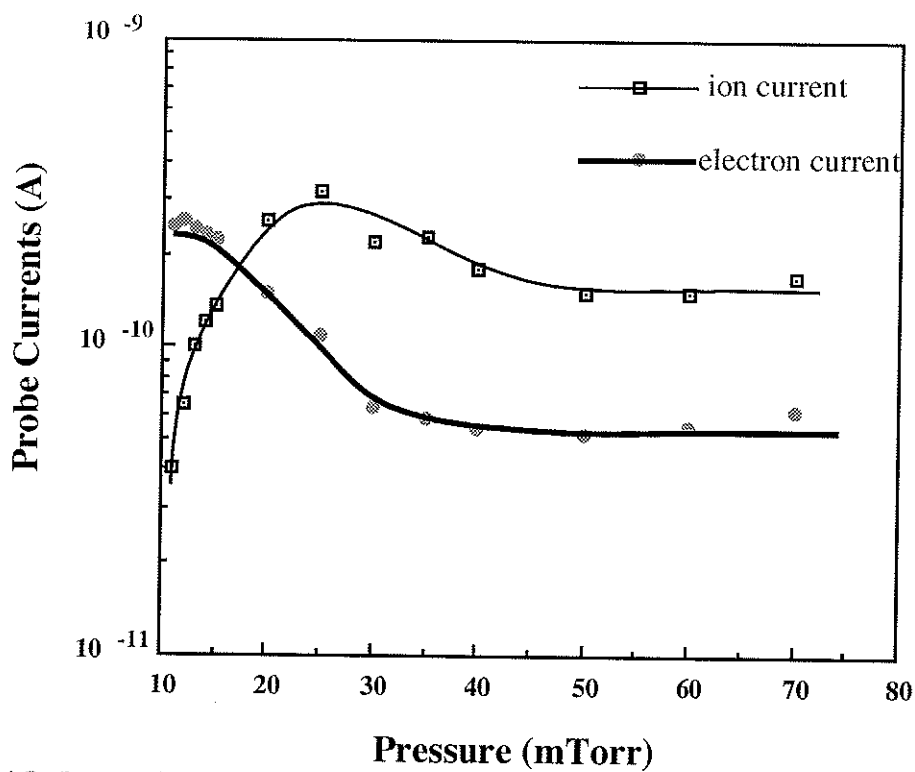


Figure 4.5 Ion and electron currents of the  $N_2O$  plasma as functions of pressure with external bias voltages of -25 V at the front grid and 25 V at the back grid (Arrangement B).

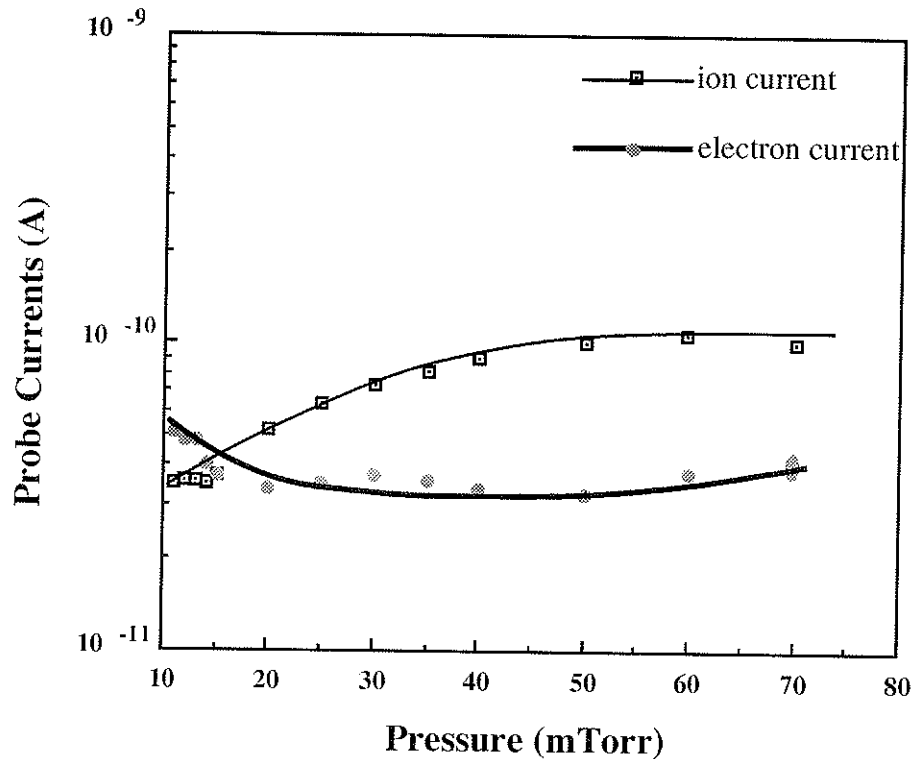


Figure 4.6 Ion and electron currents of the  $N_2O$  plasma as functions of pressure with external bias voltages of  $-40$  V at the front grid and  $40$  V at the back grid (Arrangement E).

In Fig. 4.4, both the ion current and electron current decrease with increasing gas pressure. Obviously, the currents in this case are produced by the ions and electrons in the  $N_2O$  plasma because the increase in pressure reduces the mean free path and subsequently decreases the probability of impact ionization and hence the number of the charged particles.

With bias voltages of  $25$  V and  $-25$  V at the back and the front grids, respectively, the ion and electron currents drop significantly to  $10^{-9}$  and  $10^{-10}$  A, respectively. As the pressure is increased, electron concentration behind the back grid is decreased because the mean free path decreases. As a result, more electrons collide with the gas molecules. After collisions, the electrons lose a portion of their energies and the probability for them to penetrate through the charged particle suppressor is reduced. On the other hand, the

reduction of electrons increases the effective ion concentration behind the back grid. This means that the collision between ions and gas molecules does not involve in energy exchange as much as that between electrons and gas molecules, at least for pressures between 10-80 mTorr. When the pressure is higher than 25 mTorr, the electron concentration behind the back grid saturates and a equilibrium condition is reached for both ion and electron currents.

The ion and electron currents drop to the values in the order of  $10^{-11}$  A when the front and the back grids are biased at -40 and 40 V respectively, as shown in Fig. 4.6. The ion and electron currents become saturated at pressures higher than 25 mTorr indicating that the currents are independent of the gas pressure. Therefore, the probe currents detected by the tungsten Langmuir probe is induced by photoionization but not the charged particles. We can conclude that the amount of the charged particles is obviously smaller than  $10^{-11}$  A at the bias voltage at  $\pm 40$  V. As a result, the concentration of the remaining particles in the processing chamber is small and hence the electric field near the substrate surface created by the ion sheath is small. Thus, we believe the kinetic energy of the remaining particles impinging on the substrates and the on-growing films is small and may not cause significant damage. Since the activated oxygen species which react with the reactant gas to form solid films is not affected by the biased grids, thus the amount of these species flowing to the processing chamber does not reduce.

#### **4.4 Interface Trap Density ( $D_{it}$ ) and Oxide Trapped Charge ( $Q_{ox}$ )**

The values of  $D_{it}$  and  $Q_{ox}$  as functions of bias voltages applied to the grids are shown in Table 4.2. As the dc bias voltage is higher than  $\pm 25$  V for the front and the back grids, the suppression of ions and electrons has reached its optimal condition. Therefore, we chose the bias voltage of  $\pm 40$  V. The values of  $D_{it}$  and  $Q_{ox}$  were determined from the

C-V characteristic measured after the samples had been subjected to post-metallization annealing (PMA). The C-V measurement method is shown in Appendix B.

Table 4.2 The values of  $D_{it}$  and  $Q_{ox}$  before and after photon radiation.

Charge	Remark	Without photon radiation	With photon radiation
Interface trap density ( $eV^{-1}cm^{-2}$ )	with zero bias	$7.332 \times 10^{11}$	$2 \times 10^{13}$
	with bias voltage of $\pm 40$ V	$6.068 \times 10^{11}$	$1.133 \times 10^{12}$
Oxide trapped charge ( $q\text{ cm}^{-2}$ )	with zero bias	$1.48 \times 10^{11}$	$4.6 \times 10^{11}$
	with bias voltage of $\pm 40$ V	$1.7627 \times 10^{11}$	$3 \times 10^{11}$

Table 4.2 shows that both  $D_{it}$  and  $Q_{ox}$  are affected by photon radiation. Without applying bias, the  $SiO_2$  film suffers both the ion bombardment and photon radiation and the values of  $D_{it}$  and  $Q_{ox}$  are quite high. The photon radiation increases  $D_{it}$  from  $6 \times 10^{11} \text{ eV}^{-1} \text{ cm}^{-2}$  to  $10^{12} \text{ eV}^{-1} \text{ cm}^{-2}$  and increases  $Q_{ox}$  from  $1.7 \times 10^{11} \text{ q cm}^{-2}$  to  $3 \times 10^{11} \text{ q cm}^{-2}$ . The rate of increase of  $D_{it}$  is greater than that of  $Q_{ox}$  indicating that more holes are produced in the films during photon radiation.

Photons with energies of 8-9 eV are able to create electron-hole pairs near the surface of the  $SiO_2$  film [7]. The holes tend to diffuse through the oxide and are trapped at the  $SiO_2/Si$  interface following the process [36]:



The  $SiO\bullet$  structure can act as an electron trap due to the high electron affinity of oxygen.



The  $Si\bullet$  structure can act as a hole trap due to the relatively low electron affinity of silicon.



In addition, based on the Bond Strain Gradient (BSG) model [48], the oxygen dangling bond tends to propagate in the direction of increasing strain; whereas the silicon dangling bonds stays at its original position, as shown in Fig. 4.9. Once the oxygen dangling bond arrives at the interface region, it may encounter with other Si centers and be trapped there, forming an interface trap.

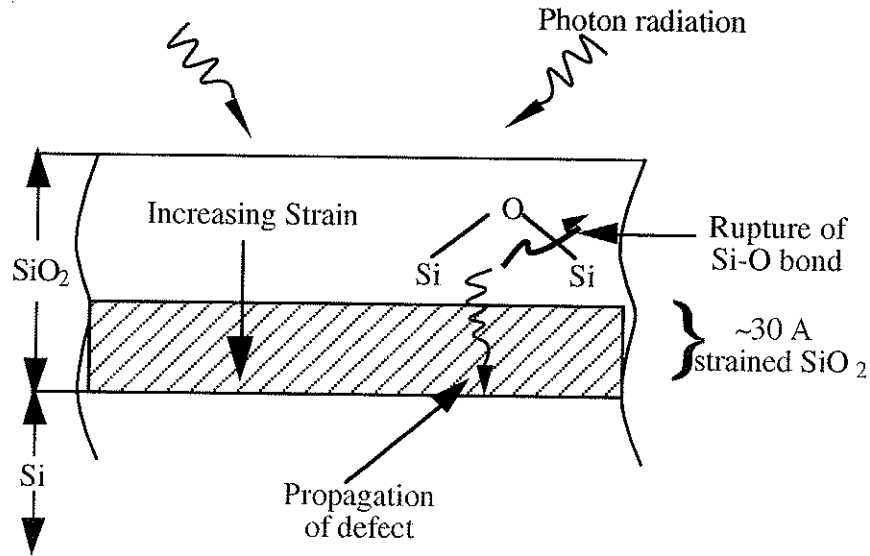


Figure 4.7 The Bond Strain Gradient model showing the rupture of the Si-O bond and the subsequent propagation of the defects toward the SiO<sub>2</sub>/Si interface.

Since electron-hole pairs are generated in SiO<sub>2</sub> upon radiation, these carriers, along with those injected from the contacts through internal photoemission, will transport through the SiO<sub>2</sub> film according to the electric field available at the time. The mobile electrons are driven out of the oxide in a very short time (~1 ps) [49]. The holes in the oxide are subjected to a further transport process. However, some holes which fall into traps inside the oxide during transport will be trapped there to form positive trapped charge; others are captured by neutral bulk traps created during ionizing radiation, leading to the accumulation of positive trapped charge. Holes which are not trapped in the bulk will proceed toward the SiO<sub>2</sub>/Si interface. Holes may also encounter electrons injected from the silicon substrate. In this case holes are subjected to a recombination process. The holes approaching the SiO<sub>2</sub>/Si interface may capture electrons from the Si substrate and create interface trap charge.

The penetrating photon radiation may also break up the bonding network of the SiO<sub>2</sub> film, which may lead to subsequent structural rearrangement. Some of the broken bonds may be able to restore their original status upon the initial electron-hole

recombination process, others may remain broken and give rise to electrically active defects. These defects are the main source for the eventual build-up of various charges and associated traps depending on their location. Moreover, the rupture of strained Si-O bonds located near the SiO<sub>2</sub>/Si interface can also result in the formation of interface traps because the non-bridging oxygen defects diffuse easily toward the interface [49]. This leaves the dangling Si bonds behind, which subsequently form the interface traps.

The bias voltage applied to the grids can suppress the ions and electrons, and thus reduce the probability of creating defects in the films. The charged particles are confined by the magnetic field around the chamber axis as shown in Fig. 4.8. The magnetic field profile is the 'thickest' right beneath the magnetic field coil. Since the substrates are placed about 8 cm from the magnetic field coil, the magnetic field profile is 'thinner' above these substrates and therefore no ion bombardment occurs even without biasing. In contrast, the substrates placed perpendicular to the chamber axis are subjected to direct bombardment by particles from the plasma and therefore the damage caused by ion bombardment is significant without biasing.

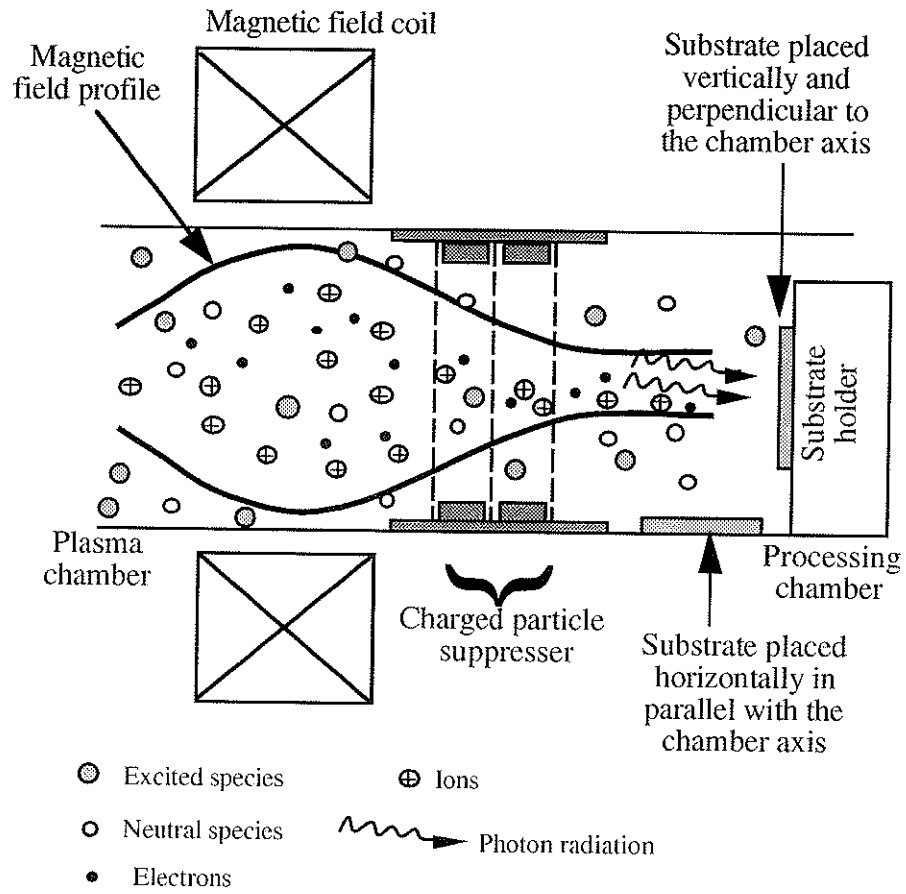


Figure 4.8 Illustration of the flow of particles and photons between the plasma and processing chamber with no bias.

## CHAPTER 5

# CONCLUSIONS

The PECVD films fabricated by ECR microwave plasmas and the photon radiation effects have been studied. On the basis of experimental work given in the previous chapters, the following conclusions are drawn:

- (1) Fluorine incorporation of the PECVD films enhances the deposition rate of the SiOF films. Fluorine acts as a 'catalyst' for the flow rate of fluorine gas below 6 sccm. As the flow rate of fluorine gas is greater than 6 sccm, fluorine acts as an etchant and tends to decrease the deposition rate.
- (2) Fluorine incorporation induces stress relaxation of the interfacial strain by the breaking of Si-O-Si bonds. The increase of fluorine incorporation results in the decrease of refractive index and subsequently the dielectric constant and polarizability of the films.
- (3) With fluorine incorporated, an increase of the flow rate of oxygen gas results in a decrease in deposition rate indicating that oxygen enhances the amount of available fluorine.
- (4) The heat treatment of SiOF films causes dissociation of Si-F bonds and desorption of atomic fluorine, which, in turn, decreases the SiF/Si-O-Si absorption peak ratio and increases the bond strain.
- (5) The XPS analysis shows that there is carbon at the outer surface of the SiOF films and its concentration drops to zero at the level deeper than 3 nm, and, on the other hand, that fluorine is bonded with silicon but not with oxygen in the SiOF films .
- (6) A suitable dc biasing applied to the grids of the charged particle suppressor prevents charged particles from bombarding the substrates and the on-growing films.
- (7) Photon radiation from the N<sub>2</sub>O plasma causes an increase in the concentration of bulk traps in the SiO<sub>2</sub> films at the SiO<sub>2</sub>/Si interface.

## REFERENCES

- [1] Y. Nishioka, E. F. Da Dilva, Jr., Y. Wang, and T. P. Ma, *IEEE Electron Device Lett.*, **9**, No.1, 38 (1988).
- [2] G. Q. Lo, W. Ting, J. H. Ahn, D. L. Kwong, and J. Kuehne, *IEEE Transactions on Electronic Devices*, **39**, No.1, 148 (1992).
- [3] U. S. Kim, C. H. Wolowodiuk, R. J. Jaccodine, F. Stevie, and P. Kahora, *J. Electrochem. Soc.*, **137**, No.7, 2291 (1990).
- [4] D. N. Kouvatso, F. A. Stevie, and R. J. Jaccodine, *J. Electrochem. Soc.*, **140**, No.4, 1160 (1993).
- [5] Y. Nishioka, K. Ohyu, Y. Ohji, N. Natuaki, K. Mukai, and T. P. Ma, *IEEE Electron Device Lett.*, **10**, 141 (1989).
- [6] E. F. Da Silva, Jr., Y. Nishioka, and T. P. Ma, *IEEE Transactions on Nuclear Science*, **NS-34**, No.6, 1190 (1987).
- [7] J. Bos and M. Hendriks, *J. Appl. Phys.*, **66**, No. 3, 1244 (1989).
- [8] P. J. Wright, and K. C. Saraswat, *IEEE Transactions on Electron Devices*, **36**, No.5, 879 (1989).
- [9] G. Q. Lo, W. Ting, D. L. Kwong, J. Kuenhe and C. Magee, *IEEE Electron Device Lett.*, **36**, No. 5, 511 (1990).
- [10] M. Seel and P.S. Bagus, *Phys. Rev. B.*, **28**, 2023 (1983).
- [11] P. G. Pai, S .S. Chao, and Y. Takagi, *J. Vac. Sci. Technol.*, **A4**, No.3, 689 (1986).
- [12] L. M. Ephrath and D. J. DiMaria, *Solid State Technol.*, 182 (1981).
- [13] T. Homma, R. Yamaguchi, and Y. Murao, *J. Electrochem. Soc.*, **140**, No.3, 687 (1993).
- [14] E. A. Irene, E. Tierney, and J. Angilello, *J. Electrochem. Soc.*, **129**, No.11, 2594 (1982).
- [15] J. L. Vossen, J. H. Thomas, III, J. -S. Maa, O. R. Mesker, and G. O. Fowler, *J. Vac. Sci. Technol.*, **A1**, No. 3, 1452 (1983).
- [16] R. E. I. Schropp, *J. Apply. Phys.*, **65**, No.9, 3706 (1989).
- [17] J. G. Huang, R. J. Jaccodine, and D. R. Young, *J. Appl. Phys.*, **75**, No.5, 2564 (1994).

- [18] D. Kouvatso, J. G. Huang, and R. J. Jaccodine, *J. Electrochem. Soc.*, **136**, No.6, 1752 (1991).
- [19] C. S. Pai, C. -P. Chang, and F. A. Baiocchi, *J. Appl. Phys.*, **68**, No.5, 2442 (1990).
- [20] A. Kazor, C. Jeynes, and I. W. Boyd, *Appl. Phys. Lett.*, **65**, No.12, 1572 (1994).
- [21] J. Batey and E. Tierney, *J. Appl. Phys.*, **60**, No.9, 3136 (1986).
- [22] L. Vishnubhotla, T. P. Ma, H. -H. Tseng, and P. J. Tobin, *IEEE Electron Device Lett.*, **14**, No.4, 196 (1993).
- [23] D. Kouvatso, F. P. McCluskey, and R. J. Jaccodine, *Appl. Phys. Lett.*, **61**, No.7, 780 (1992).
- [24] P. C. Chen, K. Y. J. Hsu, H. L. Hwang, and J. Y. Lin, *J. Appl. Phys.*, **76**, No.9, 5508 (1994).
- [25] E. V. Jelenkovic, K. Y. Tong, M. C. Poon, and J. S. L. Wong, *Semicond. Sci. Technol.*, **9**, 1673 (1994).
- [26] T. T. Chau, S. R. Mejia, and K. C. Kao, *J. Vac. Sci. Technol.*, **B10**, No.5, 2170 (1992).
- [27] T. V. Herak, T. T. Chau, D. J. Thomson, and S. R. Mejia, *J. Appl. Phys.*, **65**, No.6, 2457 (1989).
- [28] Y. Shioya, *J. Appl. Phys.*, 5102 (1987).
- [29] G. S. Viridi, C. M. S. Rauthan, B. C. Pathak, and W. S. Khokle, *Solid-State Electronics*, **34**, No.8, 889 (1991).
- [30] T. Usami, K. Shimokawa, and M. Yoshimaru, *Jpn. J. Appl. Phys.*, **33**, 408 (1994).
- [31] T. R. Oldham, F. B. Mclean, H. E. Boesch, Jr., and J. M. McGarrity, *Semicond. Sci. Technol.*, **4**, 986 (1989).
- [32] T. T. Chau, S. R. Mejia, and K. C. Kao, *Can. J. Phys.*, **69**, 165 (1991).
- [33] M. Nakamura, R. Kanzawa, and K. Sakai, *J. Electrochem. Soc.*, **133**, No.6, 1167 (1986).
- [34] W. A. Pliskin, *J. Vac. Sci. Technol.*, **14**, No.5, 1064 (1977).
- [35] W. A. Pliskin and H. S. Lehman, *J. Electrochem. Soc.*, **112**, No.10, 1013 (1965).
- [36] D. Y. Chung, *Analyses of the Annealing Processes and the Effects of Plasma Treated Substrate Surfaces for MOS Devices* (M. Sc. Thesis, University of Manitoba, 1992).

- [37] E. A. Taft, *J. Electrochem. Soc.*, **135**, 1022 (1987).
- [38] W. Kern and D. A. Puotinen, *RCA Review*, 187 (1970).
- [39] L. A. Zazzera, and J. F. Moulder, *J. Electrochem. Soc.*, **136**, No.2, 484 (1989).
- [40] J. W. Coburn, H. F. Winters, and T. J. Chuang, *J. Appl. Phys.*, **48**, No.8, 3536 (1977).
- [41] K. Ninomiya, K. Suzaki, S. Nishimatsu, and O. Okada, *J. Appl. Phys.*, **58**, 1177 (1985).
- [42] W. Y. Lee, *J. Appl. Phys.*, **51**, 3365 (1980).
- [43] R. C. Henderson, *J. Electrochem. Soc.*, **114**, 772 (1972).
- [44] T. T. Chau, *Microwave ECR Plasma Processing of Thin Film Semiconductors* (M. Sc. Thesis, University of Manitoba, 1988).
- [45] D. L. Flamm, *Solid-State Technol.*, **22**, 111 (1979).
- [46] A. C. Adams, *Solid-State Technol.*, **26**, 135 (1983).
- [47] G. E. McGuire, *Semiconductor Materials and Process Technology Handbook*, Noyes Publications, pp. 280-304 (1988).
- [48] F. J. Grunthaner, P. J. Grunthaner, and J. Maserjian, *IEEE Transactions on Nuclear Science*, **NS-29**, No.6, 1462 (1982).
- [49] A. K. W. Chan, *Radiation Effects in Metal-Oxide-Semiconductor Devices* (M. Sc. Thesis, University of Manitoba, 1993).
- [50] S. R. Kasi, M. Liehr, and S. Cohen, *Appl. Phys. Lett.*, **58**, No.25, 2975 (1991).
- [51] R. P. H. Chang, C. C. Chang, and S. Darack, *Appl. Phys. Lett.*, **36**, No.12, 999 (1980).
- [52] V. Zekeriya and T. P. Ma, *IEEE Transaction of Nuclear Science*, **NS-31**, 1261 (1984).
- [53] M. Morita, T. Kubo, T. Ishihara, and M. Hirose, *Appl. Phys. Lett.*, **45**, No.12, 1312 (1984).
- [54] D. L. Griscom, *J. Appl. Phys.*, **58**, 2524 (1985).
- [55] P. Balk, *Proceedings of the Electrochemical Society Fall Meeting* (Electrochemical Society, Buffalo, N. Y.), pp.29 (1965).
- [56] C. T. Sah, *Solid-State Electron.*, **33**, 147 (1990).

## APPENDIX A

### RCA Silicon Substrate Cleaning Process

The RCA standard clean is a two-step oxidizing treatment with hydrogen peroxide solutions. The two-step treatment consists of an alkaline mixture at high pH followed by an acidic mixture at low pH, and this is the basic framework for the RCA standard clean. The procedures are as follows:

- (1) submersion in  $\text{NH}_4\text{OH} : \text{H}_2\text{O}_2 : \text{H}_2\text{O}$  (6 : 1 : 1) at about  $80^\circ\text{C}$  for 15 minutes
- (2) deionized water rinse (with resistance of  $17.6 \text{ M}\Omega\text{-cm}$ ) for 1 minute
- (3) submersion in  $\text{HF} : \text{H}_2\text{O}$  (1 : 100) for 30 seconds
- (4) submersion in  $\text{HCl} : \text{H}_2\text{O}_2 : \text{H}_2\text{O}$  (6 : 1 : 1) at about  $80^\circ\text{C}$  for 15 minutes
- (5) deionized water rinse (with resistance of  $17.6 \text{ M}\Omega\text{-cm}$ ) for 1 minute
- (6) submersion in  $\text{HF} : \text{H}_2\text{O}$  (1 : 100) for 30 seconds

## APPENDIX B

### Capacitance-Voltage Method

#### B1. Calculation of Interface Trap Density

The high-low frequency C-V method has been used for the determination of the interface trap density. This method is superior to the high frequency C-V method alone or the quasi static (low-frequency) C-V method alone because it does not involve the computation of the theoretical C-V curves under trap free conditions. The high frequency C-V curves are usually measured at a frequency in the MHz range. At such a high frequency, the interface trap density cannot follow the small signal ac gate voltage, but follow the gate bias as the MOS capacitor is swept from the accumulation to inversion mode. The capacitance per unit area measured at a high frequency (about 1 MHz) can be written as:

$$C_{HF} = C_s C_{ox} / (C_s + C_{ox}) \quad (B1)$$

where  $C_{ox}$  is the oxide capacitance per unit area which is given by:

$$C_{ox} = \epsilon_{ox} / d \quad (B2)$$

and  $C_s$  is the depletion region capacitance which is given by:

$$C_s = \epsilon_s / W \quad (B3)$$

in which  $\epsilon_{ox}$  and  $\epsilon_s$  are the permittivities of the oxide and the silicon semiconductor, respectively and  $d$  and  $W$ , however, the oxide thickness and the depletion region depth in the silicon semiconductor, respectively.

The total capacitance at low frequencies ( $\sim 1-10$  Hz) is expressed as:

$$1/C_{LF} = 1/C_{ox} + 1/(C_s + C_{it}) \quad (B4)$$

where the ac response of the interface traps can be accounted for at these frequencies, because the response from the interface traps is immediate, which contributes to significant amount of  $C_{it}$ . Since both Eqs. (B1) and (B4) contain the  $C_s$  term, the combination of high-low frequency measurements omits the evaluation of  $C_s$ . By rearranging Eqs. (B1) and (B4), we can obtain the following expressions for the interface trap capacitance:

$$C_{it} = [1/C_{LF} - 1/C_{ox}]^{-1} - [1/C_{HF} - 1/C_{ox}]^{-1} \quad (B5)$$

However,  $C_{it}$  is:

$$C_{it}(\Psi_s) \equiv -dQ_{it}/d\Psi_s \approx q D_{it}(\phi_s) \quad (B6)$$

where  $\Psi_s$  = banding bending,  $Q_{it}$  = interface trap charge per unit area, and  $\phi_s$  = surface potential measured from intrinsic level at the silicon surface. Substituting Eq. (B5) and (B6) and solving for  $D_{it}$  yields:

$$D_{it} = 1/q \{ [1/C_{LF} - 1/C_{ox}]^{-1} - [1/C_{HF} - 1/C_{ox}]^{-1} \} \quad (B7)$$

where  $C_{HF}$  and  $C_{LF}$  denote the capacitance values at high frequency (HF) and low frequency (LF), respectively.

Extraction of the  $D_{it}$  value is often quoted at the midgap of the silicon bandgap because it is a better representation of the overall value across the silicon bandgap. This is due to the  $D_{it}$  near the band edges become less precise in describing the number of interface traps at these regions. As a result, the  $D_{it}$  values are usually obtained from the separation between the HF and the LF C-V curves in the depletion region. In order to extract this midgap value,  $D_{it}$  is converted from a function of gate bias to a function of energy level ( $E_c - E$ ) in the silicon bandgap through the following relations [49]:

$$\Psi_s(V_g) = \int_{V_{fb}}^{V_g} [1 - C_{LF}(V_g)/C_{ox}] dV_g \quad (B8)$$

$$(E_c - E)/q = E_g/2q + \Psi_s - \phi_B \quad (B9)$$

where  $V_{fb}$  = flatband voltage,  $E_c$  = conduction band edge energy,  $E$  = energy level in the gap,  $E_g$  = bandgap energy, and  $\phi_B$  = potential difference between the thermal equilibrium Fermi level and the intrinsic Fermi level in the silicon bulk. Using the above relations, we can compute the  $D_{it}$  value at midgap, which is 0.55 eV below  $E_c$  with  $E_g = 1.1$  eV for Si at room temperature.

All the capacitance values quoted above are per unit area. They are also normalized to the oxide capacitance values so that the C-V measurements will not be affected by device geometry like gate area and oxide thickness. Usage of capacitance values in the calculation of oxide charge density is also treated the same way. The LF C-V curve after normalization will be referred to as the quasi-static curve.

## B2 Calculation of Oxide Charge Density

The determination of oxide charge density ( $Q_{ox}$ ) is mainly based on the HF capacitance method. We can usually infer this density from the 'flatband voltage shift' in the HF C-V curve of the MOS device. However, in doing so, we must first locate the flatband capacitance  $C_{fb}$  and the corresponding flatband voltage  $V_{fb}$  on the C-V curves. The method is as follows:

$$C_{fb} = C_{fbs}C_{ox}/(C_{fbs} + C_{ox}) \quad (B10)$$

with

$$C_{fbs} = \sqrt{(q^2 N_D \epsilon_s/kT)} \quad (B11)$$

where  $C_{fbs}$  = silicon flatband capacitance,  $C_{ox}$  = oxide capacitance,  $N_D$  = donor concentration, and  $\epsilon_s$  = permittivity of silicon. Knowing the value of  $C_{fb}$ , we can identify the corresponding  $V_{fb}$  values from the HF C-V curves.

With the flatband voltage values determined; we can evaluate the oxide charged density by using an appropriate equation. In doing so, we can relate these values with the work function difference between the gate metal and the silicon,  $W_{ms}$ . In an ideal case, the flatband voltage is equal to  $W_{ms}$  for charge free condition at flatband. However, there is a certain amount of intrinsic oxide charge residing in the oxide film causing the apparent deviation between  $V_{fb}$  and  $W_{ms}$ , which we denote as  $V_{fb} - W_{ms}$ . This deviation is equivalent to a parallel shift of the HF C-V curve compared to the one in an ideal charge free condition. Subsequently injection or trapping of carriers can also lead to a corresponding flatband shift of the HF C-V curve. The direction of the shift is dependent on the polarity of the charge carriers. Thus, the  $Q_{ox}$  can be related to the flatband voltage shift through is as follows:

$$V_{fb} - W_{ms} = - Q_{ox}/C_{ox} = - d_{ox} Q_{ox}/\epsilon_{ox} \quad (B12)$$

where  $d_{ox}$  = oxide thickness, and  $\epsilon_{ox}$  = permittivity of the oxide in which the relation  $C_{ox} = \epsilon_{ox}/d_{ox}$  is used in the expression.